

RESEARCH

Open Access



# Suppression of the JAK/STAT pathway inhibits neuroinflammation in the line 61-PFF mouse model of Parkinson's disease

Huixian Hong<sup>1†</sup>, Yong Wang<sup>1†</sup>, Marissa Menard<sup>2†</sup>, Jessica A. Buckley<sup>1</sup>, Lianna Zhou<sup>1</sup>, Laura Volpicelli-Daley<sup>2</sup>, David G. Standaert<sup>2</sup>, Hongwei Qin<sup>1\*</sup> and ETTY N. Benveniste<sup>1\*</sup>

## Abstract

Parkinson's disease (PD) is characterized by neuroinflammation, progressive loss of dopaminergic neurons, and accumulation of  $\alpha$ -synuclein ( $\alpha$ -Syn) into insoluble aggregates called Lewy pathology. The Line 61  $\alpha$ -Syn mouse is an established preclinical model of PD; Thy-1 is used to promote human  $\alpha$ -Syn expression, and features of sporadic PD develop at 9–18 months of age. To accelerate the PD phenotypes, we injected sonicated human  $\alpha$ -Syn preformed fibrils (PFFs) into the striatum, which produced phospho-Syn (p- $\alpha$ -Syn) inclusions in the substantia nigra pars compacta and significantly increased MHC Class II-positive immune cells. Additionally, there was enhanced infiltration and activation of innate and adaptive immune cells in the midbrain. We then used this new model, Line 61-PFF, to investigate the effect of inhibiting the JAK/STAT signaling pathway, which is critical for regulation of innate and adaptive immune responses. After administration of the JAK1/2 inhibitor AZD1480, immunofluorescence staining showed a significant decrease in p- $\alpha$ -Syn inclusions and MHC Class II expression. Flow cytometry showed reduced infiltration of CD4<sup>+</sup> T-cells, CD8<sup>+</sup> T-cells, CD19<sup>+</sup> B-cells, dendritic cells, macrophages, and endogenous microglia into the midbrain. Importantly, single-cell RNA-Sequencing analysis of CD45<sup>+</sup> cells from the midbrain identified 9 microglia clusters, 5 monocyte/macrophage (MM) clusters, and 5 T-cell (T) clusters, in which potentially pathogenic MM4 and T3 clusters were associated with neuroinflammatory responses in Line 61-PFF mice. AZD1480 treatment reduced cell numbers and cluster-specific expression of the antigen-presentation genes *H2-Eb1*, *H2-Aa*, *H2-Ab1*, and *Cd74* in the MM4 cluster and proinflammatory genes such as *Tnf*, *Il1b*, *C1qa*, and *C1qc* in the T3 cluster. Together, these results indicate that inhibiting the JAK/STAT pathway suppresses the activation and infiltration of innate and adaptive cells, reducing neuroinflammation in the Line 61-PFF mouse model.

**Keywords** Parkinson's disease, Neuroinflammation,  $\alpha$ -Synuclein, JAK/STAT, AZD1480, scRNA-Seq

<sup>†</sup>Huixian Hong, Yong Wang and Marissa Menard contributed equally to this work.

\*Correspondence:  
Hongwei Qin  
hqin@uab.edu

ETTY N. Benveniste  
tika@uab.edu

<sup>1</sup>Department of Cell, Developmental and Integrative Biology, University of Alabama at Birmingham, 1918 University Boulevard, MCLM 907, Birmingham, AL 35294, USA

<sup>2</sup>Department of Neurology, University of Alabama at Birmingham, Birmingham, AL 35294, USA



## Introduction

Parkinson's disease (PD) is the most common motor neurodegenerative disorder, affecting 2–3% of the population over 65 years of age [1, 2]. Immune system dysfunction, genetic mutations, and environmental factors contribute to its pathogenesis [3], while polymorphisms in the HLA-DR (MHC Class II) locus increase risk of its development [4]. Studies show that anti-tumor necrosis factor (TNF) and nonsteroidal anti-inflammatory treatments are associated with a reduced incidence of PD symptoms [5–7].

The core pathological features of PD are neuroinflammation [8], a loss of dopamine-producing neurons, and the accumulation of misfolded, aggregated  $\alpha$ -synuclein ( $\alpha$ -Syn) in the substantia nigra pars compacta (SNpc), called Lewy pathology [1]. In postmortem tissue, Lewy pathology is associated with enhanced MHC Class II expression on microglia and infiltration of macrophages and T-cells in the midbrain [9–11]. Neuroimaging studies confirm chronic myeloid activation in the brains of PD patients [12], and increased numbers of  $\alpha$ -Syn-reactive T-cells circulating in the blood of PD patients demonstrate immune cell activation [13–15].

Research has focused on the neuroinflammatory features of PD, particularly endogenous microglia (MG) and monocytes/macrophages (MM), which infiltrate from the periphery [3, 16]. A recent study associated an increase in classical and Toll-like receptor-positive monocytes in early-moderate PD with rapid progression, greater clinical impairment, and early cognitive decline [17]. Animal models and clinical studies of PD correlate cytokine dysregulation, specifically, elevated levels of IL-6 and IFN- $\gamma$ , with the degeneration of dopamine neurons [16]. Genomic studies associate PD with mutations/variants of *LRRK2*, *MHC Class II* [18], and *PINK1* [19, 20], genes implicated in immune cell function.

Studies show that the adaptive immune system is essential to PD pathogenesis [3, 21–24]. Two major classes of lymphocytes, T-cells and B-cells, induce adaptive immunity, conferring antigen specificity and immunological memory [16]. Patients with PD have elevated numbers of CD4<sup>+</sup> and CD8<sup>+</sup> T-cells in the ventral midbrain compared to healthy controls [9]. T-cells from PD patients initiate an immune response to post-translationally modified  $\alpha$ -Syn, implicating an autoimmune reaction to intrinsic antigens [15, 21]. Moreover, a recent study associated  $\alpha$ -Syn-specific T-cell reactivity with preclinical and early PD, and pro-inflammatory CD4<sup>+</sup> T-cells are most abundant shortly after diagnosis of motor symptoms [13].

The JAK/STAT signaling pathway, in which Janus Kinases (JAKs) and Signal Transducers and Activators of Transcription (STATs) proteins interact with cytokine receptors, plays a critical role in the activation and regulation of immune responses [25, 26]. Its dysregulation (i.e., over-activation) is associated with many

pathological conditions, including multiple sclerosis (MS), rheumatoid arthritis, inflammatory bowel disease, and many cancers [27, 28]. Emerging evidence indicates that it polarizes myeloid cells and T-cells to pathogenic phenotypes [29]. We previously demonstrated that inhibiting the JAK/STAT pathway ameliorates disease severity in several preclinical models of MS [30] and reduces neuroinflammation in a PD model in which adeno-associated virus (AAV) human  $\alpha$ -Syn mediates overexpression of  $\alpha$ -Syn [31]. However, virally induced  $\alpha$ -Syn overexpression can cause up to a 30-fold increase in  $\alpha$ -Syn levels and thus does not model idiopathic PD. A pre-clinical model that better mimics PD neuroinflammatory processes is needed to define how inhibiting the JAK/STAT pathway mediates protection against neuroinflammation.

The Thy1- $\alpha$ -Syn transgenic mouse, or Line 61, uses the Thy1 promoter to express full-length, wild-type, human synuclein. It reproduces features of early PD or Dementia with Lewy Bodies, including widespread expression of  $\alpha$ -Syn, loss of dopamine terminals in the striatum, progressive changes in dopamine release in striatal content,  $\alpha$ -Syn pathology, motor and nonmotor deficits, neuroinflammation, and biochemical and molecular changes similar to those observed in PD, but with lack of neuron loss in the substantia nigra pars compacta [32, 33]. However, the mice do not develop these phenotypes until they are 9–18 months old [32, 34]. In another PD model, small, fibrillar seeds of mouse  $\alpha$ -Syn induce wild-type mice to form inclusions that biochemically and morphologically resemble those found in PD brains. However, while microglia are activated, this preformed fibril (PFF) model shows minimal expression of the MHC Class II-positive cells that characterize PD [35, 36].

Hypothesizing that introducing human PFFs into mice expressing human  $\alpha$ -Syn would better replicate human PD, we injected PFFs generated from purified, recombinant human  $\alpha$ -Syn into Line 61 mice (Line 61-PFF). Injection of hu- $\alpha$ -Syn PFFs produced  $\alpha$ -Syn inclusions in the SNpc and striatum, induced MHC Class II expression and enhanced innate and adaptive immune cell infiltration and activation in the midbrain, in contrast to injection of monomeric hu- $\alpha$ -Syn.

The Line 61-PFF model enables us to evaluate the contribution of the JAK/STAT pathway to neuroinflammatory responses, and the impact of inhibiting this pathway. Administering the JAK1/2 inhibitor AZD1480 suppressed neuroinflammation and reduced p- $\alpha$ -Syn inclusions. Single-cell RNA Sequencing (scRNA-Seq) revealed that PFF injection induced a specific monocyte/macrophage (MM) cluster expressing antigen-presentation genes and a T-cell cluster expressing numerous proinflammatory genes which correlate with neuroinflammation. Inhibiting the JAK/STAT pathway abrogated the presence of these two PFF-induced immune cell

clusters. These findings elucidate neuroinflammatory mechanisms and may inform the development of more specific therapeutic approaches and/or diagnostic biomarkers for patients with PD.

## Materials and methods

### Mice

The Thy1- $\alpha$ -Syn (Line 61) mouse overexpresses full-length, human, wild-type  $\alpha$ -Syn under the Thy-1 promoter. The model is bred by crossing female Line 61 mice with male hybrid B6D2F1 (BDF1) mice [32]. Since the transgene is inserted in the X chromosome, and random inactivation of the X chromosome carrying the mutation in female mice may occur [37], experiments used only littermate males with a Thy1- $\alpha$ -Syn-positive transgene. The University of Alabama at Birmingham (UAB) Institutional Animal Care and Use Committee approved all animal research protocols.

### Human $\alpha$ -Syn monomer and PFFs

Human monomeric  $\alpha$ -Syn (monomer) was purified using size-exclusion chromatography followed by anion exchange. The Pierce high-capacity endotoxin kit was used to remove endotoxins to  $<0.1$  EU/ $\mu$ g.  $\alpha$ -Syn PFFs were generated as described [38]. Monomer concentration was measured using A280 and the extinction coefficient of  $5960 \text{ M}^{-1}\text{cm}^{-1}$ . Monomer was diluted to 5 mg/ml in 150 mM KCl and 50 mM Tris-HCl buffer and shaken for seven days to generate PFFs. After seven days, PFF protein concentration was determined and previously noted buffer was used to bring concentration to 5 mg/ml. On the day of stereotaxic injections, PFFs were sonicated using a cup horn sonicator (QSonica) with a 15 °C water bath. Dynamic light scattering (Wyatt Technology) confirmed  $<50$  nm fragmentation of PFFs. Immediately before injection, 5 mg/ml of monomer was spun at 20,000  $\times g$ , and only the supernatant was injected to prevent aggregate formation.

### Intracranial stereotaxic injections and treatment with the JAK1/JAK2 inhibitor AZD1480

Male Line 61 mice between the age of 12–15 weeks were anesthetized using isoflurane and received stereotaxic, unilateral, intrastriatal injections using the coordinates relative to bregma: 1 mm A/P, 2 mm M/L, and  $-3.2$  mm D/V relative to the skull [38]. Those used in the flow cytometry, scRNA-Seq, and phospho-STAT experiments received bilateral intrastriatal injections for immune cell collection. Two microliters of sonicated PFFs (5 mg/ml) or monomeric  $\alpha$ -Syn (5 mg/ml) were injected at 0.5  $\mu$ l/min with a Hamilton syringe. Mice received 10 units of 1.5 mg/ml carprofen subcutaneously at the time of surgery and the following day.

Two weeks after PFF injections, Line 61-PFF mice were administered either AZD1480 by oral gavage at 25 mg/kg or 0.1% DMSO (Sigma-Aldrich) as a vehicle control every day. The mice were sacrificed two or four weeks later (four- or six-weeks post injection [wpi]), depending on the analysis performed. For examination of TH positive neurons, the mice were sacrificed at a 12-week time point. At time of sacrifice, they were transcardially perfused with cold PBS (pH 7.4), followed by 4% paraformaldehyde for immunofluorescence or cold PBS alone for other experiments.

### Immunofluorescence and immunohistochemistry

Prior to sectioning, brains were postfixed in 4% PFA overnight at 4 °C, followed by cryoprotection in 30% sucrose/PBS until tissues sank to the bottom. Whole brains were frozen in N-methylbutane at  $-50$  °C. Coronal Sect. 40- $\mu$ m thick representing the entire brain were serially collected and stored in 50% glycerol in 0.01% sodium azide in Tris-buffered saline (TBS) at  $-20$  °C.

Immunofluorescence analysis of free-floating brain sections was performed as previously detailed [31]. Sections were then labeled with anti-MHC Class II [A-I/A-E] (clone M5/114.15.2, Invitrogen, cat #14-5321-85), anti-phospho- $\alpha$ -Synuclein (p- $\alpha$ -Syn) (phospho-Serine129, clone EP1536Y, Abcam, cat #ab51253), anti-tyrosine hydroxylase (TH, Abcam, cat #ab76442), anti-IBA1 (polyclonal, Wako, cat #019-197111) or anti-p-STAT3 (phospho-Y705, Abcam, cat #ab76315) antibodies. After overnight incubation with primary antibodies, sections were washed and incubated with the appropriate Alexa-fluor-conjugated secondary antibodies (Life Technologies). Sections were mounted onto positively charged glass slides and cover-slipped using Prolong Gold (ThermoFisher). Images were acquired using either a Leica TCS-SP5 laser scanning confocal microscope or a Nikon Ti2-C2 confocal microscope and processed using Adobe Photoshop and Illustrator [38]. The immunofluorescence intensity was quantified using Fiji [31].

Free-floating immunohistochemistry was performed as detailed previously [39]. Brain sections were labeled with anti-tyrosine hydroxylase (Millipore, ab152), a marker of dopaminergic neurons in mouse midbrain. On day two the sections were labeled with a biotinylated secondary followed by HRP-conjugated amplification complex. DAB chromogenic substrate deposition was timed and visualized by eye (Vector, SK-4100) before mounting on positively charged slides, which were dehydrated and cover-slipped using Permount (Fisher, SP15-500).

### Unbiased stereology

To quantify TH neurons in the SNpc, unbiased stereology was performed as described [39]. A reviewer blinded to condition coded and analyzed 5–6 TH-DAB-stained

slides encompassing the rostro caudal SNpc using an Olympus BX51 microscope and the optical fractionator probe in the StereoInvestigator software (MBF Bioscience). Both ipsilaterally injected and contralaterally uninjected sides of the SNpc were quantified. TH<sup>+</sup> neurons within the SNpc contours on a 100  $\mu\text{m}$  x 100  $\mu\text{m}$  grid were counted at an optical dissector height of 22  $\mu\text{m}$ . Weighted section thickness was used to account for variations in tissue thickness. Brightfield images of TH<sup>+</sup> neurons in the SNpc were acquired using the Olympus BX51 microscope.

#### Phospho-synuclein aggregate quantitation

After immunofluorescence staining with anti- $\alpha$ -phospho-Serine129 (p- $\alpha$ -Syn) as described [38, 40], 20X tiled, ipsilateral SNpc confocal images were obtained using the Nikon Ti2-C2 microscope. An ImageJ cell counter was used to count each p- $\alpha$ -Syn-positive neurite and inclusion in the SNpc, which was delineated by drawing a contour using TH<sup>+</sup> neurons as a reference and then splitting the channels so only p- $\alpha$ -Syn channel fluorescence remained. Two to six SNpc sections were analyzed per animal, depending on their availability and quality after staining.

#### Mononuclear cell isolation

Six weeks after bilateral injection of monomer or PFFs, mononuclear cells in the ventral midbrain were isolated as described [31, 41]. Midbrain tissue was passed through a 100- $\mu\text{m}$  filter to obtain a single-cell suspension, and mononuclear cells were isolated using a 30/70% Percoll gradient.

#### Flow cytometry

To detect surface proteins, mononuclear cells were incubated with Fc Block (Bio X Cell, 2.4G2) for 15 min and washed, followed by incubation with viability dye. The indicated antibodies were fluorescently conjugated against CD45 (clone 30-F11, BD Horizon, cat #563410), CD11b (clone M1/70, BD Biosciences, cat #563553), CD11c (clone HL3, BD Pharmingen, cat #553801), CD4 (clone GK1.5, BioLegend, cat #100428), CD8 $\alpha$  (clone 53-6.7, BioLegend, cat #100734), CD19 (clone 6D5, BioLegend, cat #115541), and MHC Class II (clone M5/114.15.2, BioLegend, cat #107628). Samples were run on a BD Symphony (BD Biosciences) and analyzed using FlowJo software (Tree Star), as described [31, 41, 42].

#### Immunoblotting

Thirty  $\mu\text{g}$  of midbrain mononuclear cell homogenate was separated by electrophoresis and probed with antibodies, including p-STAT1, STAT1, p-STAT3, STAT3 and GAPDH, as described [30]. All immunoblots represent three individual experiments. Fold-induction of p-STAT1,

STAT1, p-STAT3, and STAT3 were calculated by normalizing to GAPDH, with the monomer sample set as 1.0. The ratios of p-STAT1:STAT1 and p-STAT3:STAT3 were also calculated using ImageJ 1.53t [30].

#### Single-cell RNA sequencing (scRNA-Seq)

Mononuclear cells were isolated for sequencing as described above with 3–5 ventral midbrains pooled per sample and sorted for CD45<sup>+</sup> live cells on a BD FACSAria. Sorted cells were loaded onto the 10X Chromium platform (10X Genomics), and libraries constructed using the Single Cell 3' Reagent Kit V3.1 according to the manufacturer's instructions. At least three biological replicates for each group were processed separately (PBS [ $n=3$ ], monomer [ $n=3$ ], PFF+vehicle [ $n=4$ ], PFF+AZD1480 [ $n=5$ ]). Samples were sequenced at an average depth of 20,000 reads per cell using Illumina NextSeq 500. Raw base call files were demultiplexed into FASTQ files. Sequencing files were processed and mapped to mm10, and count matrices were extracted using the Cell Ranger Single Cell Software (v 7.1.0) [43].

#### scRNA-seq analysis

The count matrices in the h5 file format were imported into the Partek Flow (Partek, Inc.) pipeline [44]. Single-cell quality control was performed by applying an inclusion filter on counts per cell (500–15000) and detected genes per cell (250–5000). Cells with more than 10% mitochondrial gene expression were excluded to eliminate apoptotic or dying cells [45]. The noise-reduction filter was also applied to exclude features where the value  $\leq 0$  is in at least 99.9% of cells. The filtered dataset was normalized and scaled with SCTransform workflow.

Principal component analysis (PCA) was performed on the SC-scaled data to graph clustering based on the Louvain algorithm, with the PCA number set to 20. The data were visualized by 3D uniform manifold approximation and projection (UMAP) dimensional reduction using the first 20 principal components. Cell annotations for each cluster were determined using the top differentially expressed genes (DEGs) in computed biomarkers and canonical markers following the classification workflow in Partek Flow [46]. Differences in gene expression among samples were determined by the Hurdle model on log<sub>2</sub> normalized counts. Dot and violin plots were generated with `sc.pl.dotplot` and `sc.pl.violin` functions in Scanpy (1.9.1) [47] using annotated h5ad files exported from Partek workflow.

The MM1 and MM2 clusters were subsets of the original annotated data node in Partek. They were reclustered as MM1 to MM5 following standard PCA and graph-based processes on SCTransform-scaled data and visualized with UMAP. The T-cell cluster was a subset of the

original annotated data node in Partek and reclustered as T1 to T5 [48].

### Pathway enrichment analysis

GSEA (gene set enrichment analysis): DEG between individual MG, MM, or T clusters was determined via the Partek gene-specific analysis (GSA) test. The exported DEG list was ranked by  $-\log(P)$  and converted to an RNK file uploaded to GSEA software (version 4.3.2, BROAD Institute). GSEAPreRanked chooses a hallmark gene-set database [49]. Pathway analysis results were plotted in terms of a normalized enrichment score (NES) and a false discovery rate (FDR) using the ggplot2 (version 3.4.0) package in RStudio.

### Statistical analysis

Flow cytometry experiments used 3–5 independent samples per group, with two ventral midbrains per sample (6–10 mice per experiment). Data were analyzed using an unpaired t-test (two-tailed) between two groups or one-way ANOVA between more than two independent groups. Graphs display the individual values and mean  $\pm$  SD, with  $*p < 0.05$ ,  $**p < 0.01$ ,  $***p < 0.001$ , and  $****p < 0.0001$ .

### Data set availability

ScRNA-Seq data will be available online. The single-cell data have been deposited in the GEO under the accession number GSE264525. Raw files supporting our findings are available from the corresponding authors upon reasonable request.

## Results

### Novel pre-clinical PD model (line 61-PFF)

We previously showed that the JAK1/2 inhibitor AZD1480 prevents neuroinflammation and protects against dopaminergic neuron loss in response to AAV-human- $\alpha$ -Syn overexpression in rats [31]. To better mimic idiopathic PD, we tested mouse PFFs and found that injection into mouse striatum activated microglia but did not induce the accumulation of MHC Class II-expressing immune cells (data not shown) that occur in human PD brains [50]. We therefore tested whether injecting *human*  $\alpha$ -Syn PFFs into the striatum of Line 61 mice, which use the Thy1 promoter to express human  $\alpha$ -Syn [32], would induce more robust inflammatory phenotypes. Using an antibody to  $\alpha$ -Syn phosphorylated at serine 129 (p- $\alpha$ -Syn), we identified  $\alpha$ -Syn inclusions in the SNpc four weeks after injecting Line 61 mice with human PFFs (Fig. 1A and B). We also observed abundant MHC Class II-positive immune cells in the SNpc (Fig. 1A and C). Injecting monomeric  $\alpha$ -Syn into Line 61 mice did not produce p- $\alpha$ -Syn inclusions or MHC Class II-positive cells (Fig. 1A), which align with previous studies on

rats injected with monomer, as conducted by our group [38, 51, 52]. Therefore, we omitted quantification of the monomer group in Fig. 1B and C.

We tested the JAK1/2 inhibitor AZD1480 in the Line 61-PFF model as described [31]. Two weeks after PFF injections, AZD1480 or VH was administered for two weeks, then mice were sacrificed for immunofluorescence studies. Figure 1A, B and C show that AZD1480 treatment significantly reduced p- $\alpha$ -Syn inclusions ( $p = 0.048$ ) and the number of MHC Class II-positive cells ( $p = 0.032$ ) in the SNpc.

Sections from the SNpc were stained for TH to determine the number of dopaminergic neurons in mice injected with monomer or PFFs and treated with VH or AZD1480. Line 61-PFF mice did not exhibit a loss of TH-positive neurons compared to monomer-injected mice at a 12-week time point, and AZD1480 treatment produced no significant differences (Supplemental Fig. 1A and 1B).

### Neuroinflammation in line 61-PFF mice

Injecting human PFFs into the striatum of Line 61 mice increased MHC Class II positive immune cells in the SNpc, and AZD1480 treatment reduced the abundance of these cells (Fig. 1). Immune cell phenotypes in the midbrain were further characterized by flow cytometry (Fig. 2A and B). In Line 61-PFF mice, total immune cells in the midbrain were significantly higher ( $p = 0.014$ ) than in monomer  $\alpha$ -Syn-injected mice (Fig. 2C). We identified microglia as  $CD45^{Mid}CD11b^{+}$ , macrophages as  $CD45^{Hi}CD11b^{+}$ , dendritic cells (DCs) as  $CD45^{Hi}CD11b^{+}CD11c^{+}$ , and lymphocytes as  $CD45^{+}CD11b^{-}$ . In Line 61-PFF mice, macrophages ( $p = 0.011$ ), DCs ( $p = 0.045$ ), and lymphocytes ( $p = 0.0008$ ) showed significant increases compared to monomer-injected mice, but the total number of microglia did not increase (Fig. 2C).

We assessed the activation status of innate immune cell subsets by determination of MHC Class II expression. Absolute numbers of MHC Class II positive microglia ( $p = 0.031$ ), macrophages ( $p = 0.020$ ), and DCs ( $p = 0.033$ ) were significantly higher in the midbrain of Line 61-PFF mice than in the monomer group (Fig. 2D).

Since adaptive immune cells are also implicated in PD [3, 21–24], we determined how pathologic  $\alpha$ -Syn affects infiltration of  $CD4^{+}$  T-cells,  $CD8^{+}$  T-cells, and  $CD19^{+}$  B-cells. We found a significant increase in  $CD19^{+}$  B-cell ( $p = 0.014$ ) but not  $CD4^{+}$  or  $CD8^{+}$  T-cell infiltration in Line 61-PFF mice compared to the monomer group, although  $CD4^{+}$  T-cell infiltration trended towards significance ( $p = 0.07$ ) (Fig. 2E).

We next determined how AZD1480 treatment influenced specific subsets of immune cells (Fig. 2A and B). AZD1480 or VH was administered two weeks after PFF injections, and treatment continued for four weeks,

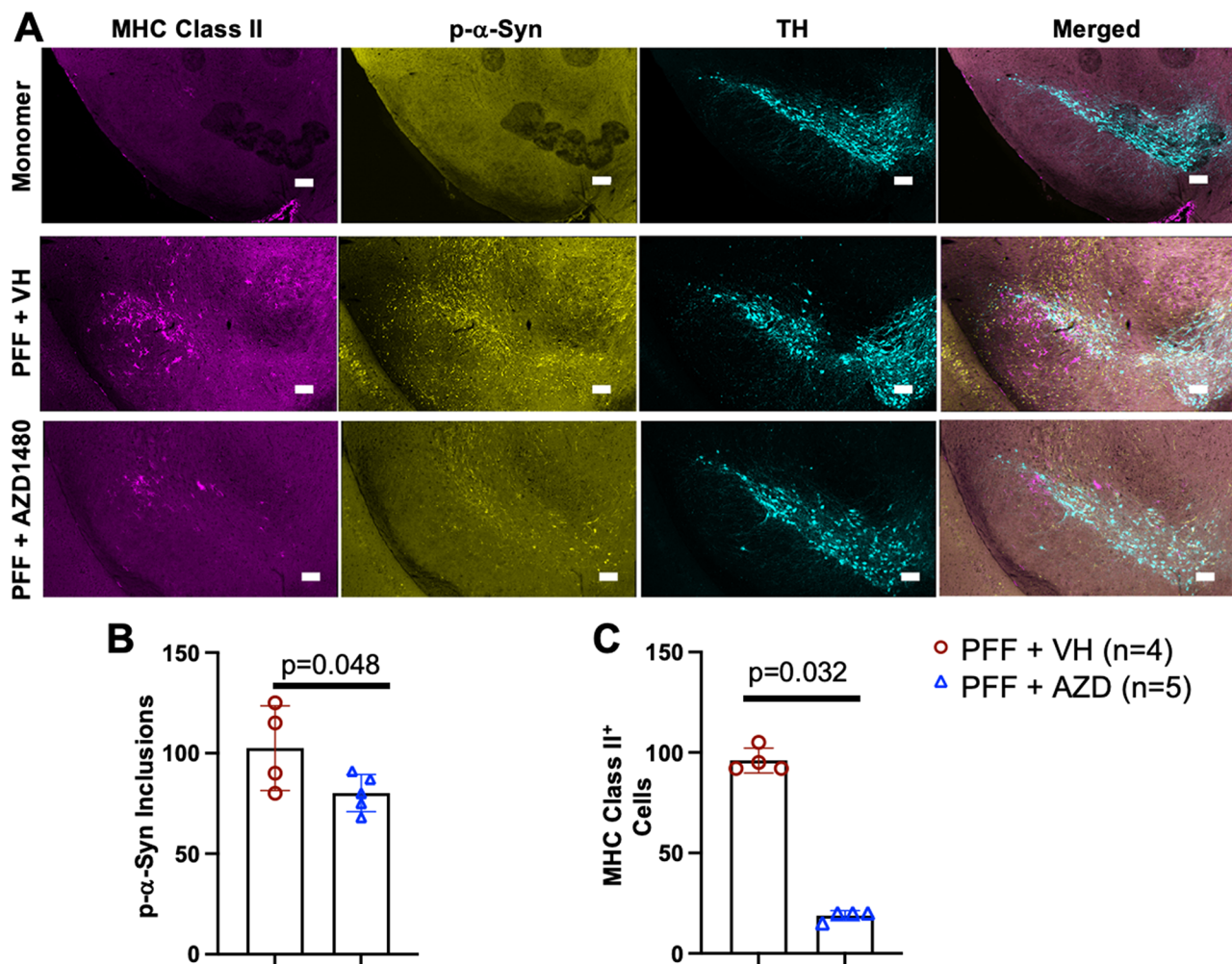


**Fig. 1** Increased MHC Class II Expression and  $\alpha$ -Syn Phosphorylation in Line 61-PFF Mice. Male Line 61 mice (12–15 weeks old) were unilaterally injected in the striatum with human  $\alpha$ -Syn monomer (10  $\mu$ g) or hPFF (PFF) (10  $\mu$ g). Four weeks later, those injected with human  $\alpha$ -Syn monomer were perfused for immunofluorescence. Two weeks later, those injected with hPFF, were treated with VH (DMSO) or AZD1480 (25 mg/kg/day) for an additional two weeks for a total of four weeks. **(A)** Immunofluorescence performed in the SNpc detected MHC Class II (magenta), phospho- $\alpha$ -Syn (p- $\alpha$ -Syn) (yellow), or TH (cyan). The abundance of MHC Class II-positive cells or p- $\alpha$ -Syn inclusions was quantified using Fiji. **(B)** An independent t-test showed significant differences in the number of MHC Class II-positive cells between VH- and AZD1480-treated groups. **(C)** An independent t-test showed significant differences in the number of p- $\alpha$ -Syn-positive aggregates between groups. Scale bar = 100  $\mu$ m. \* $p < 0.05$

when mice were sacrificed for analysis. Compared to VH, AZD1480 significantly suppressed absolute numbers of immune cells (microglia ( $p=0.025$ ), macrophages ( $p=0.010$ ), DCs ( $p=0.035$ ), and lymphocytes ( $p=0.0007$ ), the numbers of MHC Class II positive microglia ( $p=0.0005$ ), macrophages ( $p=0.0002$ ) and DCs ( $p=0.007$ ), and the number of CD4<sup>+</sup> T-cells ( $p=0.0001$ ), CD8<sup>+</sup> T-cells ( $p=0.0071$ ), and CD19<sup>+</sup> B-cells ( $p=0.0003$ ) in the midbrain of Line 61-PFF mice (Fig. 2C, D and E). These data show that inhibiting the JAK/STAT pathway suppresses the infiltration and activation of innate and adaptive immune cells.

#### PFF induction of STAT3 activation

Activation of the JAK/STAT pathway results in phosphorylation of STAT proteins [28]. We assessed activation in Line 61-PFF mice by measuring tyrosine phosphorylation of STATs, particularly STAT1 and STAT3 [30, 53]. Immunoblotting was performed to measure protein expression levels of total STAT1, phosphorylated STAT-1 (p-STAT1), total STAT3, and p-STAT3 in mononuclear cells isolated from the midbrain. We observed a significant increase in p-STAT3 in Line 61-PFF mice treated with VH compared to monomer ( $p=0.0149$ ), which was inhibited by AZD1480 treatment ( $p=0.0128$ ) (Fig. 3A and B). To confirm the results on p-STAT3, the ratio of p-STAT3:STAT3 was calculated. This demonstrates a significant increase in Line 61-PFF mice treated with VH

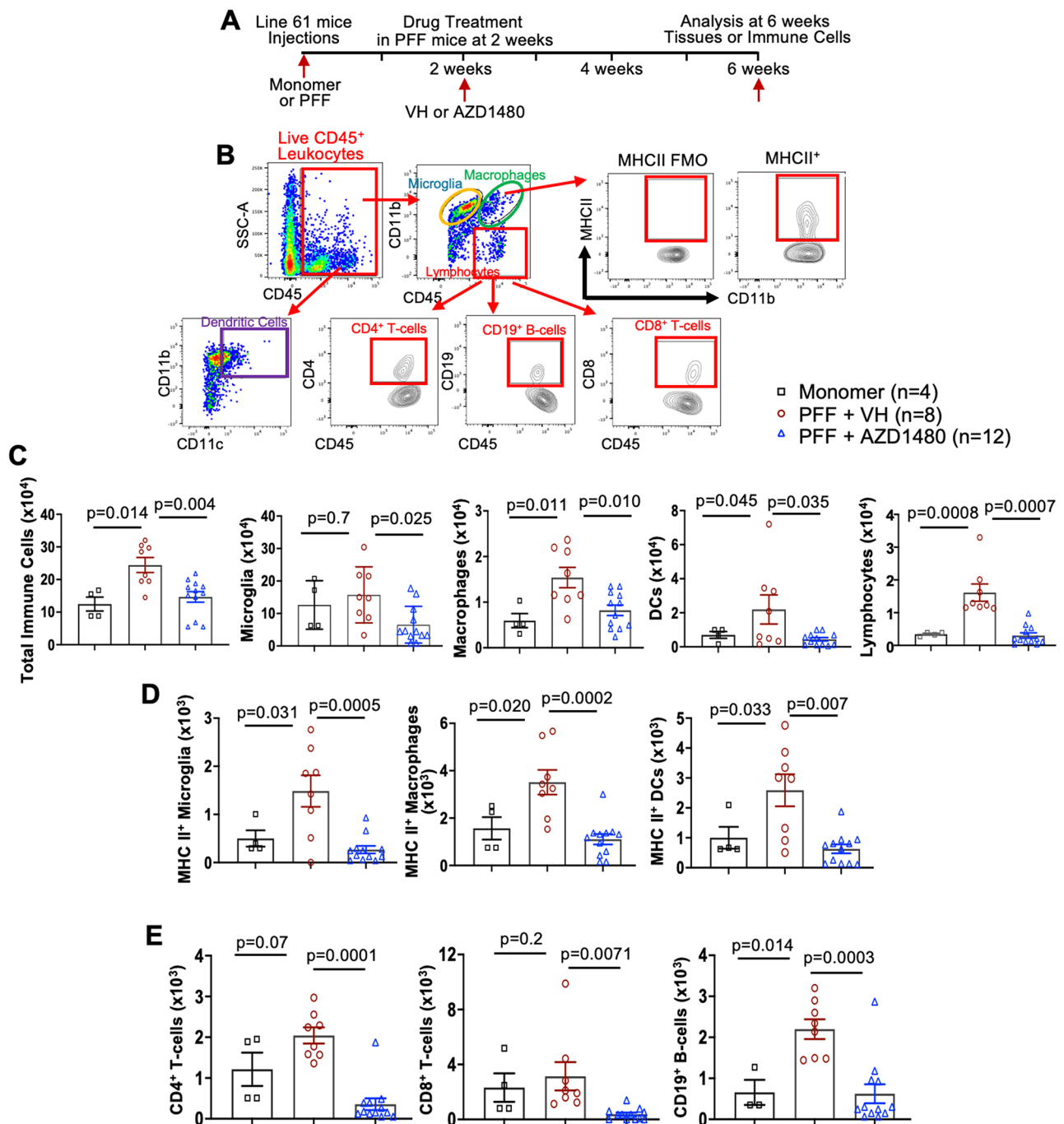


**Fig. 2** Experimental Design, Gating Strategy, and Flow Analysis of Innate and Adaptive Immune Cells from the Midbrain. **(A)** Male Line 61 mice (12–15 weeks old) were bilaterally injected in the striatum with monomer (10 μg) or PFF (10 μg). Two weeks after PFF injection, VH (DMSO) or AZD1480 (25 mg/kg/day) was administered by oral gavage for an additional four weeks for a total of six weeks. **(B)** Mononuclear cells were isolated from midbrains. The gating strategy of flow cytometry analysis was as follows: CD45<sup>Med</sup>CD11b<sup>+</sup> microglia, CD45<sup>Hi</sup>CD11b<sup>+</sup> macrophages, CD45<sup>Hi</sup>CD11b<sup>+</sup>CD11c<sup>+</sup> dendritic cells (DCs), CD45<sup>+</sup>CD11b<sup>-</sup>CD4<sup>+</sup> T-cells, CD45<sup>+</sup>CD11b<sup>-</sup>CD8<sup>+</sup> T-cells, and CD45<sup>+</sup>CD11b<sup>-</sup>CD19<sup>+</sup> B-cells. Representative gating plots of MHC Class II expression in microglia, macrophages, and DCs are shown. Fluorescence minus one (FMO) was used as a control. **(C)** Six weeks post injection, mononuclear cells were isolated from the midbrains of monomer (n=4), PFF+VH (n=8), or PFF+AZD1480 (25 mg/kg/day) (n=12) mice, then subjected to flow cytometry analysis. Absolute numbers of total CD45<sup>+</sup> immune cells, CD45<sup>Med</sup>CD11b<sup>+</sup> microglia, CD45<sup>Hi</sup>CD11b<sup>+</sup> macrophages, CD45<sup>+</sup>CD11b<sup>+</sup>CD11c<sup>+</sup> DCs, and CD45<sup>+</sup>CD11b<sup>-</sup> lymphocytes are shown as mean ± SD. **(D)** Absolute numbers of MHC Class II-positive CD45<sup>Med</sup>CD11b<sup>+</sup> microglia, macrophages, and DCs are shown as mean ± SD. **(E)** Absolute numbers of CD4<sup>+</sup> T-cells, CD8<sup>+</sup> T-cells, and CD19<sup>+</sup> B-cells are shown as mean ± SD. Statistical significance was determined by ordinary one-way ANOVA. \*p < 0.05, \*\*p < 0.01, \*\*\*p < 0.001

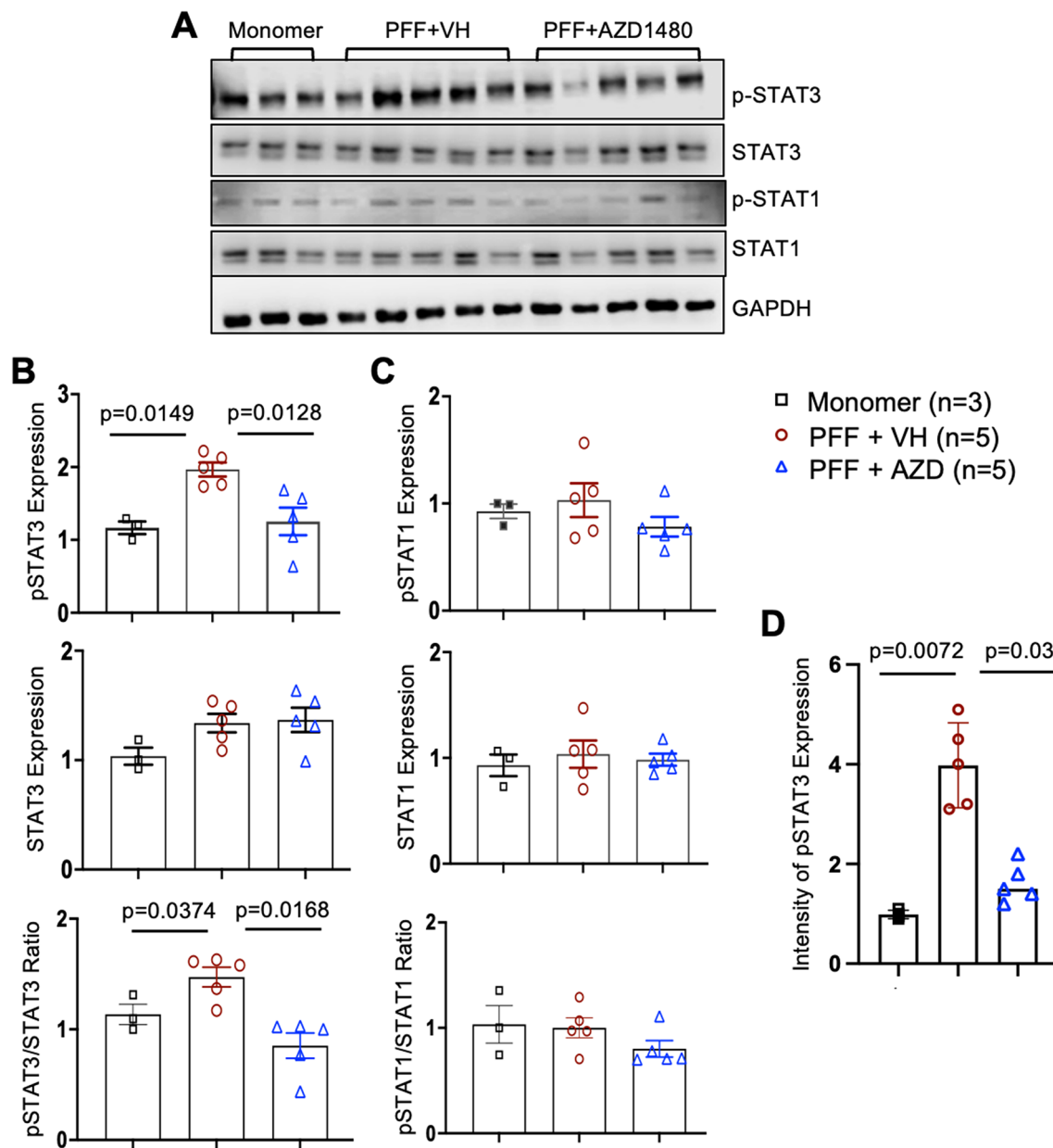


**Fig. 3** AZD1480 Inhibits PFF-induced STAT3 Phosphorylation in the Midbrain. **A.** Male Line 61 mice (12–15 weeks old) were bilaterally injected in the striatum with monomer (10  $\mu$ g) or PFF (10  $\mu$ g). Two weeks after PFF injection, VH or AZD1480 (25 mg/kg/day) was administered by oral gavage for an additional four weeks. Lysates were obtained from mononuclear cells isolated from the midbrains of monomer ( $n=3$ ), PFF+VH ( $n=5$ ), or PFF+AZD1480 ( $n=5$ ) mice at six weeks and immunoblotted with the indicated antibodies. **B.** Fold-induction of p-STAT3 and total STAT3 was calculated by normalizing to GAPDH; and the ratio of p-STAT3 to total STAT3 using ImageJ 1.53t. **C.** Fold-induction of p-STAT1 and total STAT1 was calculated by normalizing to GAPDH; and the ratio of p-STAT1 to total STAT1 using ImageJ 1.53t. **D.** Quantification of p-STAT3 levels in the SNpc (4 sections/sample) by immunofluorescence staining in monomer ( $n=3$ ), PFF+VH ( $n=5$ ), or PFF+AZD1480 ( $n=5$ ) mice six weeks post injection. Statistical significance was determined by ordinary one-way ANOVA. \* $p < 0.05$ , \*\* $p < 0.01$

compared to monomer ( $p=0.0374$ ) and that AZD1480 treatment suppressed this ratio ( $p=0.0168$ ) (Fig. 3B). There were no statistical differences in total STAT3, total STAT1 and p-STAT1 protein expression and the p-STAT1:STAT1 ratio (Fig. 3A, B and C). Immunofluorescence staining confirmed the significant increase in p-STAT3<sup>+</sup> cells in Line 61-PFF mice treated with VH

compared to monomer treatment ( $p=0.0072$ ), and suppression after AZD1480 treatment ( $p=0.03$ ) (Fig. 3D and Supplemental Fig. 2). These data indicate that PFF injection activates the JAK/STAT pathway as demonstrated by phosphorylated STAT3, and AZD1480 inhibits STAT3 activation in mononuclear cells.



### scRNA-Seq characterization of immune cell clusters in line 61-PFF mice

Several scRNA-Seq studies point to the heterogeneity of cells involved in PD pathogenesis [54–57]. To identify cell-specific contributions in the Line 61-PFF model, we performed scRNA-Seq on sorted CD45<sup>+</sup> leukocytes obtained from Line 61 mice injected with PBS, monomer, PFF plus VH, or PFF plus AZD1480 (Supplemental Fig. 3). Cell clusters were annotated with the top differentially expressed biomarkers and canonical markers for microglia (MG), monocytes/macrophages (MM), T-cells (T), B-cells (B) and neutrophils (Neu) (Supplemental Fig. 4A). We observed no difference in the percentage of each cluster or total cell numbers between the PBS and monomer groups, indicating that monomer injection did not affect the immune cell subsets found in PBS-treated Line 61 mice (Supplemental Fig. 4B and 4C). Most cells (>80%) were identified as MG and separated into 9 clusters (MG1-9; Supplemental Fig. 4A). Upon PFF injection, either the percentage or absolute numbers of MG2, MG4, and MG5 clusters were higher than those in PBS- and monomer-injected mice (Supplemental Fig. 4B, 4C, 4F and 4G). Percentages and cell numbers of MM clusters and the T-cell cluster were higher in PFF injected mice than in PBS- and monomer-injected mice (Supplemental Fig. 4B, 4C, 4F and 4G). Neu and B-cell clusters were not examined due to low (<1%) numbers (Supplemental Fig. 4F and 4G).

### scRNA-seq reveals an PFF-induced MM inflammatory cluster which is modulated by AZD1480 treatment

We found no differences in MM cell cluster percentage or numbers between the PBS and monomer groups (Supplemental Fig. 4B and 4C). To further characterize MM clusters, we used the original annotated dataset to recluster MM1 and MM2 as MM1 - MM5 (Supplemental Fig. 4D). MM1, MM2, and MM3 were the major clusters identified in the monomer group (Fig. 4A and B). Examining their transcriptional profiles, *Gng10* and *Ldhd* were highly expressed in the MM1 cluster, while genes related to antigen presentation, *H2-Eb1*, *H2-Aa*, *H2-Ab1*, and *Cd74* [58, 59], were enriched in MM2 and MM4 (Supplemental Fig. 5A and 5B). Genes related to macrophage function and signal transduction, including *F13a1*, *Cd163*, *Mrc1*, *Ms4a7*, and *Pf4* [60] were differentially expressed in MM3, while *Nav2*, *Nav3*, *Ldlrad4*, *Dennd4a*, and *Csm3*, genes associated with Alzheimer's Disease, Autism Spectrum Disorders (ASD), aging, axon guidance and signal transduction [61–66] were elevated in MM4. Only MM5 expressed *Nfib*, *Dnm3*, and *Fermt2* (Supplemental Fig. 5A and 5B). GSEA revealed that the MM2 and MM4 clusters were enriched in IFN- $\alpha$  and IFN- $\gamma$  responses, IL-6-JAK-STAT3 signaling, TNF- $\alpha$  signaling

via NF- $\kappa$ B, Hedgehog signaling, inflammatory responses and hypoxia (Supplemental Fig. 5C).

We examined whether the MM clusters changed with PFF injection. MM1, MM2, MM3, and MM4 cell numbers increased in Line 61-PFF mice compared to monomer, with the MM4 cluster showing the greatest increase (Fig. 4A and B), and DEG analysis revealed upregulated expression of MM4 genes (Fig. 4C).

AZD1480 treatment reduced MM2, MM3, and MM4 cell numbers, almost eliminating the MM4 cluster, and increased MM1 cell numbers (Fig. 4B). *H2-Eb1*, *H2-Aa*, *H2-Ab1*, and *Cd74* genes were suppressed in the MM2 and MM4 clusters (Fig. 4C and D) and *Nav2*, *Csm3*, *Nav3*, *Ldlrad4*, and *Dennd4a* in the MM4 cluster (Fig. 4C). Collectively, these results suggest that MM4 is a potentially pathogenic cluster that emerges after PFF injection, and AZD1480 treatment abrogates the appearance of the MM4 cluster.

### AZD1480 treatment reduces MG Cluster cell numbers but does not influence transcriptional profiles in line 61-PFF mice

Microglia play a critical role in PD pathogenesis [67–69], so we assessed their transcriptional profiles in Line 61 mice. MG1, MG3, MG4, and MG6 were the major MG clusters found in the PBS and monomer groups, with no differences in the percentage or cell numbers of the 9 MG clusters (Supplemental Fig. 4B and 4C). All MG clusters expressed the canonical gene markers *P2ry12* and *Cx3cr1*. MG1 strongly expressed *Klf2* and *Egr3*, MG3 expressed *Maf* and *Slc2a5*, and MG5 expressed *Spp1* and *ApoE*. Although MG2 primarily upregulated *Gm42418* and *Cmss1*, and MG4, *Gng10* and *Alox5ap*, neither does so exclusively. MG6 upregulated two genes, *Snx29* and *Anks1*, and downregulated *Maf* and *Slc2a5*. The MG7 cluster upregulated *Stat3* and *Cd83* and downregulated *Klf2* and *Egr3*. MG8 expressed *Top2a* and *Mki67*, and MG9 uniquely expressed *Ifit2*, *Ifit3*, *Oasl*, and *Irf7* (Supplemental Fig. 6A and 6B). GSEA revealed that the MG2 and MG9 clusters were enriched in IFN- $\alpha$  and IFN- $\gamma$  response pathways, and MG2 was also enriched in TGF- $\beta$  and PI3K-AKT-MTOR signaling (Supplemental Fig. 6C).

PFF injection increased MG2, MG4, MG5, MG8, and MG9 cell numbers compared to monomer injection (Fig. 5A and B), with MG2 showing the greatest increase. However, PFF injection did not change transcriptional profiles to any great extent (Fig. 5C). While AZD1480 treatment reduced cell numbers of MG1, MG4, MG5, MG8, and MG9 clusters overall and MG2 cell numbers to the low levels seen in monomer mice (Fig. 5B), DEG analysis identified only subtle changes in *Gm42418*, *Cmss1*, *ApoE*, and *Actb* (Figs. 5C and 6D).

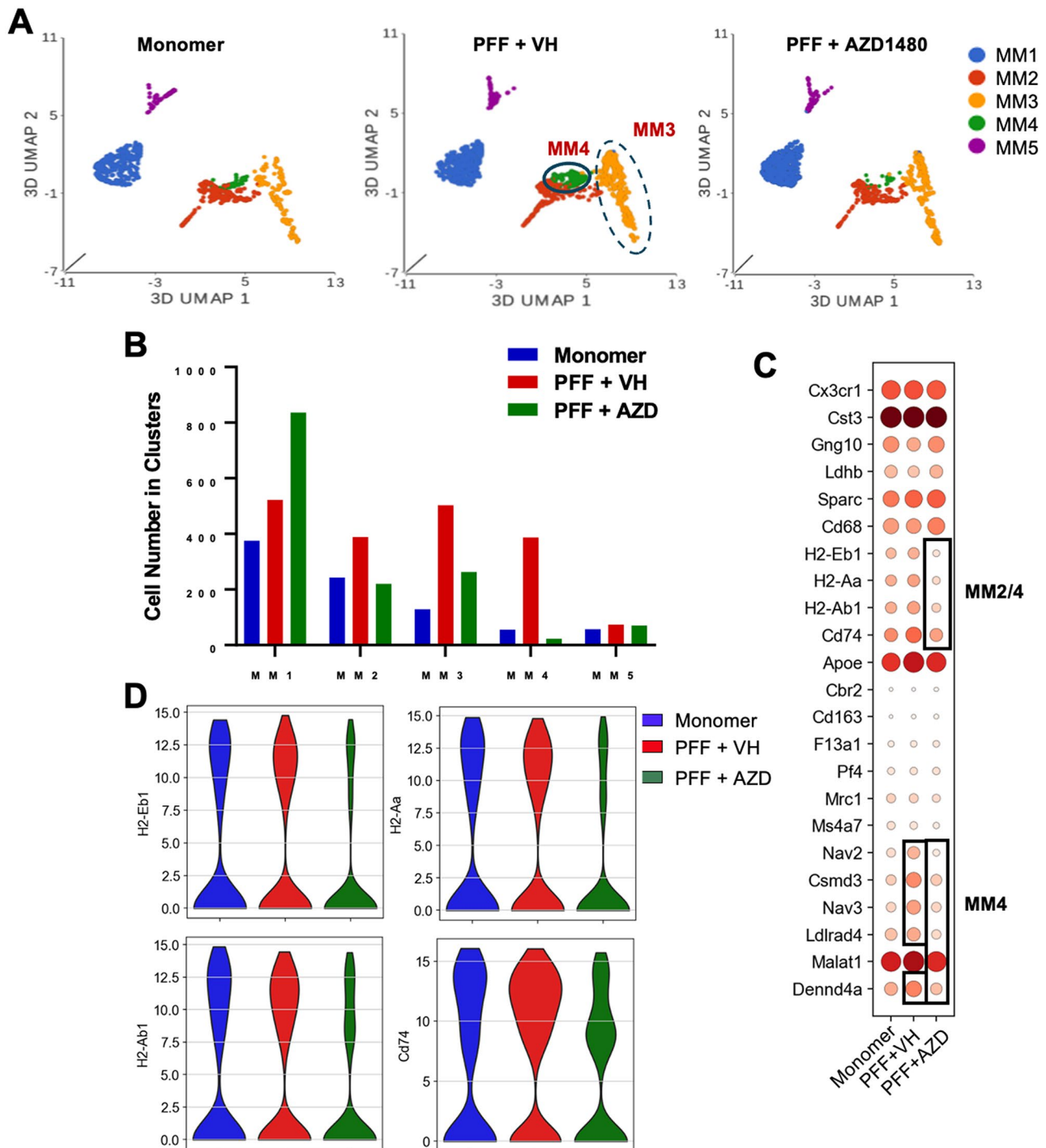


**Fig. 4** scRNA-Seq Reveals an PFF-induced MM Inflammatory Cluster Which is Modulated by AZD1480 Treatment. **(A)** UMAP visualization of MM clusters from monomer, PFF + VH, or PFF + AZD1480 (25 mg/kg/day) bilaterally injected mice. **(B)** Cell numbers of the five MM clusters analyzed by scRNA-Seq. **(C)** Dot plot of conserved marker genes in the five MM clusters across groups. **(D)** Violin plots showing the expression-level distribution of MHC Class II genes across groups

**scRNA-seq reveals an PFF-induced T-cell inflammatory cluster which is modulated by AZD1480 treatment**

We identified five T-cell clusters (T1 to T5) (Fig. 6A and Supplemental Fig. 4A and 4E). Most of the T-cells in monomer-treated mice were in cluster T1, which

strongly expressed *Cd3e*, *Cd3d*, *Cd3g*, and *Trac*, genes encoding the T-cell receptor (TCR) [70]. The T2 cluster expressed *Ncr1*, *Xcl1*, *Klrb1b*, and *Klrb1c*; T4, *Gzma* and *Klri2*; and T5, *Gata3*, a gene related to Th2 differentiation

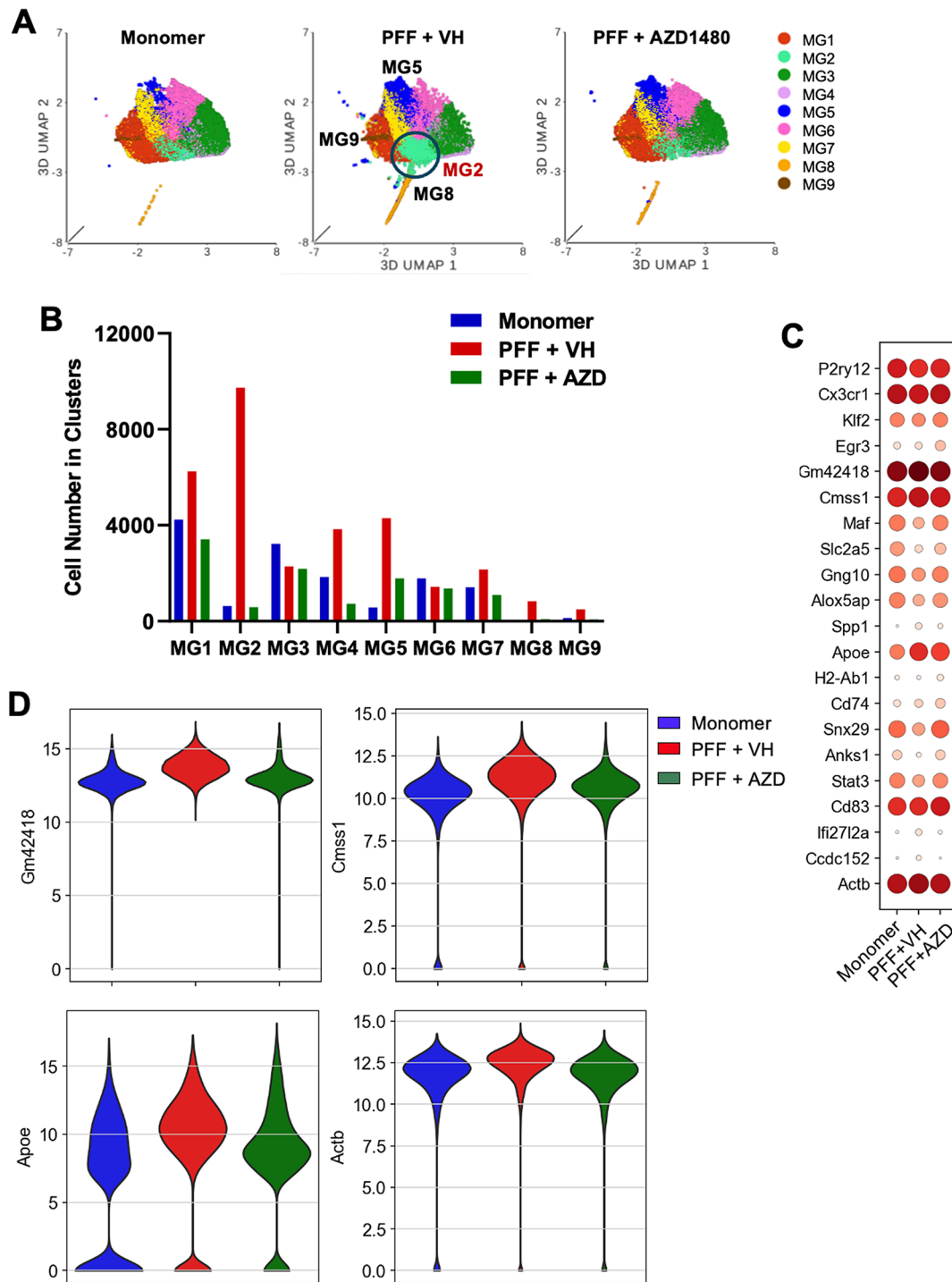


**Fig. 5** AZD1480 Treatment Reduces Cell Numbers but Does Not Influence MG Clusters' Transcriptional Profiles in Line 61-PFF Mice. **A.** UMAP visualization of MG clusters from monomer, PFF +VH, or PFF + AZD1480 (25 mg/kg/day) mice. **B.** Cell numbers of the nine MG clusters analyzed by scRNA-Seq. **C.** Dot plot of conserved marker genes in the nine MG clusters across groups. **D.** Violin plots showing the expression-level distribution of genes related to inflammatory responses across groups

[71, 72] (Supplemental Fig. 7A and 7B). Strikingly, PFF injection uniquely induced a new cluster, T3, which most strongly expressed numerous proinflammatory genes, including *Cst3*, *Csmd3*, *C1qc*, *C1qa*, *Cd83*, *Tnf*, and *Il1b*

(Fig. 6A and B; Supplemental Fig. 7A, 7B and 7C). GSEA revealed that the T2 and T4 clusters were enriched in the IFN- $\gamma$  response pathway and IL-2-STAT5 pathway, while PI3K-AKT-MOTR, IL-6-JAK-STAT3, TNF- $\alpha$  signaling

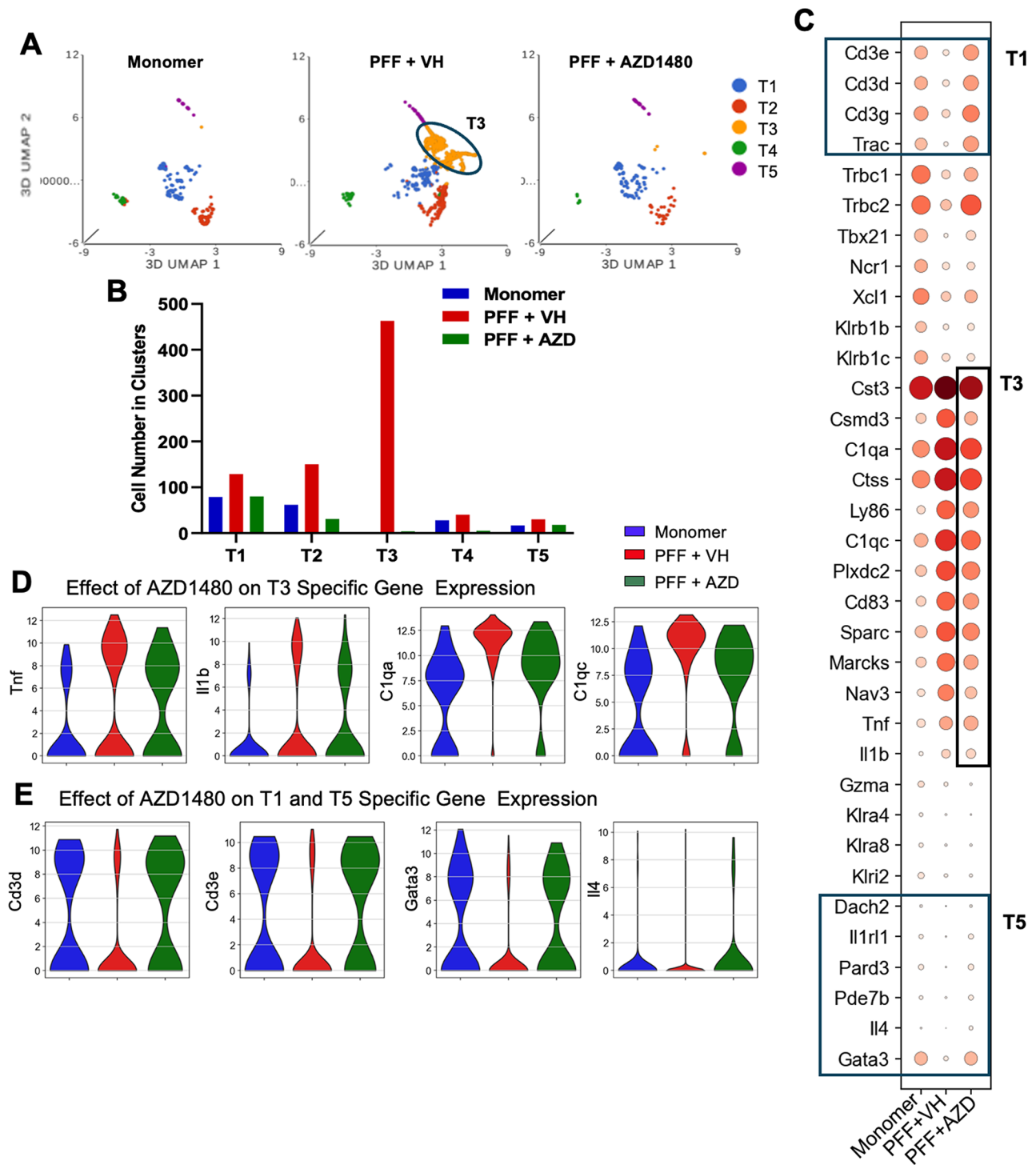


**Fig. 6** T-cell Clusters Associated with PFF-induced Neuroinflammation and the Influence of AZD1480 Treatment. **(A)** Unsupervised clustering of scRNA-Seq data and UMAP plot of all T-cells (T) from CD45<sup>+</sup> mononuclear cells sorted from the midbrain of Line 61 mice after monomer, PFF + VH, or PFF + AZD1480 injection. **(B)** Cell numbers of the five T-cell clusters analyzed by scRNA-Seq. **(C)** Dot plot of conserved marker genes in the five T-cell clusters across groups. **(D)** Violin plots show the genes restored by AZD1480 treatment in the T3 cluster across groups. **(E)** Violin plots showing genes restored by AZD1480 treatment in the T1 and T5 clusters across groups

via NF- $\kappa$ B and Notch signaling were enhanced in the T5 cluster (Supplemental Fig. 7E). The T3 cluster showed enriched Myc-target signaling (Supplemental Fig. 71E). Cell numbers in the T1 and T2 clusters were increased by PFF injection, and as mentioned previously, the T3 cluster emerged only after PFF injection (Fig. 6B).

AZD1480 treatment reduced T1 and T2 cell numbers, with an almost complete abrogation of the T3 cluster (Fig. 6A and B). *Tnf*, *Il1b*, *C1qa*, and *C1qc* gene expression was also reduced upon AZD1480 treatment (Fig. 6C and D). Interestingly, AZD1480 restored expression of the naïve T-cell-related genes *Cd3e*, *Cd3d*, *Cd3g* and *Trac* [73, 74] in the T1 cluster as well as the Th2-related genes *Gata3* and *Il4* [75] in the T5 cluster (Fig. 6C and E; Supplemental Fig. 7A, 7B and 7D). Other T-cell related genes, *Trbc1*, *Trbc2* and *Tbx21*, were also restored upon AZD1480 treatment (Fig. 6C).

Collectively, these results reveal that a novel inflammatory T-cell cluster, T3, is induced in response to PFF injection, and is associated with neuroinflammatory responses. AZD1480 treatment significantly decreased T3 cell numbers and suppressed proinflammatory gene expression. AZD1480 also restored T1 and T5 transcriptional profiles, suggesting that the JAK/STAT pathway affects T-cells in the Line 61-PFF model of PD.

## Discussion

Developing a pre-clinical model of PD that closely resembles human PD is crucial in understanding the mechanisms that influence onset and progression of the disease and identifying potential therapeutic targets. We have generated a new pre-clinical PD model by injecting human PFF into Line 61 mice that utilize the thyl promoter for expression of wild-type human  $\alpha$ -Syn. This model, Line 61-PFF, is characterized by increased expression of MHC Class II and infiltration and activation of innate and adaptive immune cells in the mid-brain, thereby exhibiting a strong neuroinflammatory response. We utilized single-cell transcriptomics, a powerful research tool that enables high-resolution analysis of gene expression [46, 76–78] to evaluate the transcriptional profiles of immune cells infiltrating into the mid-brain of Line 61-PFF. Most strikingly, we identified two unique clusters, MM4 and T3, that were induced by PFF injection. A JAK1/2 inhibitor, AZD1480, was used to investigate the effect of blocking the JAK/STAT pathway on neuroinflammation. Our results revealed an immunosuppressive effect of JAK1/2 inhibition by reducing immune cell infiltration in the brain, and inhibiting proinflammatory transcriptional profiles. These findings indicate the therapeutic potential of JAK/STAT blockade in the treatment of neurodegenerative diseases with pronounced neuroinflammation.

To define the heterogeneity of immune cells involved in neuroinflammation in Line 61-PFF mice, scRNA-Seq was utilized. We identified 5 monocyte/macrophage (MM) clusters and a significant effect of PFF injection on the MM4 cluster, enhancing expression of the antigen-presentation genes *H2Eb1*, *H2-Aa*, *H2-Ab1*, and *Cd74* as well as genes related to neurological diseases and pro-inflammatory M1 polarization, including *Nav2*, *Nav3*, *Malat1*, *Csmd3*, *Ldlrad4*, and *Dennd4a* [61–66]. Neuron navigator 2 (*Nav2*) is highly expressed in patients with rheumatoid arthritis (RA); it is considered a pathogenic gene for RA [79], and STAT3 activation has been shown to upregulate its expression in RA synoviocytes [80]. Several single-nucleotide polymorphisms (SNPs) in the *Nav2* gene are associated with the risk and age at onset of AD [81]. Note that STAT3 is activated in Line 61-PFF mice (Fig. 3), and AZD1480 treatment suppresses *Nav2* expression in the MM4 cluster (Fig. 4C). In addition, GSEA revealed that the MM4 cluster was enriched in TNF- $\alpha$  signaling (Supplemental Fig. 51C), and TNF- $\alpha$  has been shown to significantly increase *Nav2* expression [79]. In Line 61-PFF mice, we found enriched *Tnf* gene expression in the PFF-induced T3 cluster (Supplemental Fig. 7A and 7 C), suggesting that the increase in MM4 *Nav2* expression may be induced by T3-derived TNF- $\alpha$ . The expression of CUB and Sushi multiple domains 3 (*Csmd3*) and neuron navigator 3 (*Nav3*), genes related to ASD [61–64], is also elevated in the MM4 cluster and suppressed by AZD1480 treatment (Fig. 4C).

Recent studies demonstrated that monocyte-derived disease inflammatory macrophages (DIMs) accumulate during aging, inflammation, and AD [82–84]. The DIM-conserved transcriptional signature includes genes such as *Il1a*, *Il1b*, *Tnf*, *Cd49f*, *Cd54* and *Cd83* [82]. The MM4 cluster induced by PFF injection expresses many of these genes. Enrichment analysis identified that the MM4 cluster was enriched in inflammatory response, ROS signaling, and TNF- $\alpha$  signaling pathways (Supplemental Fig. 5C), indicating a pro-inflammatory phenotype. These observations indicate the MM4 cluster identified in Line 61-PFF mice exhibits inflammatory gene signatures of DIMs [82]. Importantly, AZD1480 treatment abrogated the presence of the MM4 cluster. These findings identify the MM4 cluster as a potential therapeutic target for PD.

The MM3 cluster identified in Line 61-PFF mice resemble the disease-activated border-associated macrophages (DaBAMs) identified in another  $\alpha$ -Syn model of PD [60]. Both are characterized by high expression of genes such as *Cd163*, *F13a1*, *Pf4*, *Mrc1*, *Ms4a7*, and *ApoE*. ApoE mediates neuroinflammation and neurodegeneration in AD [85, 86]. The *APOE* genotype directly influences the development of  $\alpha$ -synuclein pathology in PD dementia [87, 88]. Mouse models of  $\alpha$ -synucleinopathy showed that *APOE4* exacerbated  $\alpha$ -synuclein pathology

in the absence of amyloid [89, 90]. *ApoE* expression was elevated in the MM3 cluster (Supplemental Fig. 5A) and suppressed by AZD1480 treatment (Fig. 4C). Collectively, our results point to MM4 and MM3 as potentially pathogenic clusters and demonstrate that AZD1480 treatment inhibits proinflammatory gene expression to reduce neuroinflammation.

Studies demonstrate the essential role of T-cells in the neuropathogenesis of PD [9, 15, 16, 21] and associate  $\alpha$ -Syn-specific, proinflammatory CD4<sup>+</sup> T-cell reactivity with preclinical and early PD [13]. Several scRNA-Seq studies have focused on T-cells isolated from the blood and cerebrospinal fluid of PD patients, demonstrating the differentiation and expansion of peripheral CD8<sup>+</sup> T-cells and CD4<sup>+</sup> T-cells, as well as the interaction of peripheral CD4<sup>+</sup> T-cells with endothelial cells in PD patients [56, 91, 92]. A recent snRNA-Seq study revealed an increased frequency of T-cells within the SNpc from postmortem PD patients [55]. However, little is known about the transcriptional features of T-cells in PD, especially T-cells infiltrating the CNS. We identified increased percentages and numbers of T-cell clusters in Line 61-PFF mice (Supplemental Fig. 4; Fig. 6A and 6B). Wang et al. revealed activated and expanded T-cell populations in the blood of PD patients compared to healthy controls [92]. The T-cell cluster 11 in their study was enriched in *KLRB1* (kill cell lectin like receptor B1) expression with clonal expansion in the blood. Our scRNA-Seq analysis showed that the T2 cluster had elevated expression of *Klrb1b* and *Klrb1c* (orthologous to human *KLRB1*), which resembles the human T-cell cluster C11 in peripheral blood of patients with PD [92]. Another scRNA-Seq study using human PD peripheral blood showed that PD-associated cytotoxic CD4<sup>+</sup> T-cells exhibited a significant increase in proportion and enhancement of IFN- $\gamma$  responses [56]. Consistent with this finding, GSEA demonstrated that the IFN- $\gamma$  response pathway was enriched in T2 and T4 clusters from Line 61-PFF mice (Supplemental Fig. 7E).

Our scRNA-Seq analysis demonstrated a novel PFF-induced T-cell cluster, T3, which specifically expressed proinflammatory genes, including *Cst3*, *Csmd3*, *C1qc*, *Tnf*, and *Il1b*. AZD1480 treatment abolished the T3 cluster (Fig. 6B) and, surprisingly, restored the naïve T-cell cluster (T1) as well as expression of the Th2-related genes *Gata3* and *Il-4* in the T5 cluster (Fig. 6E). *Il4* and *Gata3* are critical for the differentiation of CD4<sup>+</sup> Th2 cells, which have immunosuppressive functions [71, 72]. Interestingly, idiopathic PD patients show low *Gata3* mRNA levels [93], consistent with another study reporting significantly few Th2 cells in PD patients [94]. IL-4 attenuates the inflammatory responsiveness of macrophages, which limits inflammasome activation, IL-1 $\beta$  production, and pyroptosis [95]. We surmise that JAK inhibition may promote immunosuppressive functions in adaptive

T-cells. However, the exact role of Th2 cells, *Gata3*, and *Il-4* in PD remains largely unknown. The JAK-STAT pathway has a critical role in the fate of T helper cell (Th) differentiation [26, 96]. STAT3 plays a crucial role in T-cell pathogenicity, promoting inflammatory responses [97–100]. In Line 61-PFF mice, STAT3 is activated in mononuclear cells from the midbrain, which may lead to the promotion of proinflammatory T-cells. AZD1480 treatment reduced STAT3 activation, which was associated with reduced neuroinflammation and abrogation of the T3 cluster.

In Line 61 mice, there is considerable pathology at 9–18 months of age, including accumulation of  $\alpha$ -Syn, loss of dopamine terminals in the striatum, microglial and astrocytic activation, elevation of inflammatory markers and CD4<sup>+</sup> T-cell infiltration into the brain [37, 101]. In Line 61-PFF mice, we observed a much earlier demonstration of  $\alpha$ -Syn inclusions and neuroinflammatory responses at 4–6 weeks. However, no TH positive neuronal loss was observed in this model at 12 weeks following PFF injection, thus we were not able to assess the impact of inhibiting the JAK/STAT pathway on the neurodegenerative process. Future studies will require examination of longer time points or the use of other models with significant dopamine neuron loss in the SNpc to determine if neurodegeneration can be influenced by JAK/STAT pathway inhibition.

## Conclusion

In summary, studies in the novel Line 61-PFF model, which displays a strong neuroinflammatory response, identified two specific immune cell clusters, MM4 and T3, that express high levels of genes related to antigen presentation and neuroinflammation. We also showed the clinical potential of inhibiting the JAK/STAT pathway critical to immune cell infiltration and expression of signature genes in these pathogenic macrophage and T-cell clusters. Future studies targeting these genes/clusters may inform diagnostic markers and/or therapeutic approaches to prevent or ameliorate currently incurable neuroinflammatory and neurodegenerative diseases, such as PD.

## Abbreviations

AAV	Adeno-associated virus
$\alpha$ -Syn	$\alpha$ -synuclein
Csmd3	CUB and Sushi multiple domains 3
DaBAMs	Disease-activated border-associated macrophages
DCS	Dendritic cells
DEGs	Differential expressed genes
DIMs	Disease inflammatory macrophages
FDR	False discovery rate
GSEA	Gene set enrichment analysis
JAK	Janus Kinases
KLRB1	Kill cell lectin like receptor B1
MG	Microglia
MM	Monocyte/macrophage
MS	Multiple sclerosis

Nav2	Neuron navigator 2
Nav3	Neuron navigator 3
NES	Normalized enrichment score
Neu	Neutrophils
p- $\alpha$ -Syn	phosphor-Syn
PCA	Principal component analysis
PD	Parkinson's disease
PFF	Performed fibril
RA	Rheumatoid arthritis
scRNA-Seq	Single-cell RNA Sequencing
SNpc	Substantia nigra pars compacta
snRNA-Seq	Single-nucleus RNA Sequencing
STAT	Signal Transducers and Activators of Transcription
TNF	Tumor necrosis factor
UMAP	Uniform manifold approximation and projection
VH	Vehicle

## Supplementary Information

The online version contains supplementary material available at <https://doi.org/10.1186/s12974-024-03210-8>.

Supplementary Material 1

## Acknowledgements

This work was supported by National Institutes of Health (NIH) grants P50NS108675 (to DGS, ENB, LVD) and AG075057 (to HQ). We thank the UAB Flow Cytometry & Single Cell Core Facility for assistance with the flow cytometry and scRNA-Seq experiments. The Core is supported by the Center for AIDS Research, NIH A1027767, and the O'Neal Comprehensive Cancer Center, NIH CA013148. We thank Drake Thrasher for his technical assistance.

## Author contributions

H.H.; Y.W.; M.M.; J.A.B.; L.Z.; L.V.D.; and H.Q. have no financial conflicts of interest to declare. D.G.S. is a member of the faculty of the University of Alabama at Birmingham and is supported by endowment and University funds. DGS is an investigator in studies funded by AbbVie, the American Parkinson Disease Association, The Michael J. Fox Foundation for Parkinson Research, Alabama Department of Commerce, Alabama Innovation Fund, the Department of Defense, and NIH (P50NS108675, R25NS079188, and T32NS095775). DGS has a clinical practice and is compensated for these activities through the University of Alabama Health Services Foundation. In addition, since January 1, 2021, he has served as a consultant for or received honoraria from AbbVie, Sutter Health, Curium Pharma, Appello, Theravance, Sanofi-Aventis, Alnylam Pharmaceuticals, Coave Therapeutics, BlueRock Therapeutics, and F. Hoffman-La Roche. E.N.B. is a member of the faculty of the UAB and is supported by endowment and University funds. She is an investigator in studies funded by The Michael J. Fox Foundation for Parkinson Research, the Department of Defense (W81CWH-18-1-0036), and NIH (P30CA013148-49, P50NS108675, R01NS109529, R01CA246708, R01AI148711, and R01DK122986-02). In addition, since January 1, 2021, she has served as a consultant for or received honoraria from the SONTAG Brain Tumor Foundation, The Race to Erase MS Foundation, the NIH, the American Association for Medical Colleges, The National Multiple Sclerosis Society, and Emory University.

## Funding

H.H., Y.W., M.M., J.A.B., L.Z., L.V.D., D.G.S., H.Q., and E.N.B. was supported by National Institutes of Health (NIH) grants P50NS108675. L.Z., H.Q., and E.N.B. was supported by National Institutes of Health (NIH) AG075057.

## Data availability

scRNA-Seq data will be available online. The single-cell data have been deposited in the GEO under the accession number GSE264525. Raw files supporting our findings are available from the corresponding authors upon reasonable request.

## Declarations

### Ethical approval

All animal experiments were performed according to all applicable laws and regulations on the protection of animals used for scientific purposes after receiving approval for the animal license (IACUC-20015) from the University of Alabama at Birmingham (UAB) Institutional Animal Care and Use Committee.

### Competing interests

The authors declare no competing interests.

Received: 22 April 2024 / Accepted: 26 August 2024

Published online: 01 September 2024

## References

- Poewe W, Seppi K, Tanner CM, Halliday GM, Brundin P, Volkman J, Schrag AE, Lang AE. Parkinson disease. *Nat Rev Dis Primers*. 2017;3:17013.
- Kalia LV, Lang AE. Parkinson's disease. *Lancet*. 2015;386:896–912.
- Harms AS, Yang YT, Tansey MG. Central and peripheral innate and adaptive immunity in Parkinson's disease. *Sci Transl Med*. 2023;15:eak3225.
- Klingenhoefer L, Reichmann H. Pathogenesis of Parkinson disease—the gut-brain axis and environmental factors. *Nat Rev Neurol*. 2015;11:625–36.
- Peter I, Dubinsky M, Bressman S, Park A, Lu C, Chen N, Wang A. Anti-tumor necrosis factor therapy and incidence of Parkinson Disease among patients with inflammatory bowel disease. *JAMA Neurol*. 2018;75:939–46.
- Gagne JJ, Power MC. Anti-inflammatory drugs and risk of Parkinson disease: a meta-analysis. *Neurology*. 2010;74:995–1002.
- San Luciano M, Tanner CM, Meng C, Marras C, Goldman SM, Lang AE, Tolosa E, Schule B, Langston JW, Brice A, Corvol JC, Goldwurm S, Klein C, Brockman S, Berg D, Brockmann K, Ferreira JJ, Tazir M, Mellick GD, Sue CM, Hasegawa K, Tan EK, Bressman S, Saunders-Pullman R. Nonsteroidal anti-inflammatory use and LRRK2 Parkinson's Disease penetrance. *Mov Disord*. 2020;35:1755–64. and J. F. F. L. C. C. Michael.
- Tansey MG, Wallings RL, Houser MC, Herrick MK, Keating CE, Joers V. Inflammation and immune dysfunction in Parkinson disease. *Nat Rev Immunol*. 2022;22:657–73.
- Brochard V, Combadiere B, Prigent A, Laouar Y, Perrin A, Beray-Berthet V, Bonduelle O, Alvarez-Fischer D, Callebert J, Launay JM, Duyckaerts C, Flavell RA, Hirsch EC, Hunot S. Infiltration of CD4+ lymphocytes into the brain contributes to neurodegeneration in a mouse model of Parkinson disease. *J Clin Invest*. 2009;119:182–92.
- Galiano-Landeira J, Torra A, Vila M, Bove J. CD8 T cell nigral infiltration precedes synucleinopathy in early stages of Parkinson's disease. *Brain*. 2020;143:3717–33.
- Williams GP, Schonhoff AM, Jurkuvenaite A, Gallups NJ, Standaert DG, Harms AS. CD4 T cells mediate brain inflammation and neurodegeneration in a mouse model of Parkinson's disease. *Brain*. 2021;144:2047–59.
- Belloli S, Morari M, Murtagh V, Valtorta S, Moresco RM, Gilardi MC. Translation imaging in Parkinson's Disease: focus on neuroinflammation. *Front Aging Neurosci*. 2020;12:152.
- Lindestam Arlehamn CS, Dhanwani R, Pham J, Kuan R, Frazier A, Rezende Dutra J, Phillips E, Mallal S, Roederer M, Marder KS, Amara AW, Standaert DG, Goldman JG, Litvan I, Peters B, Sulzer D, Sette A. Alpha-synuclein-specific T cell reactivity is associated with preclinical and early Parkinson's disease. *Nat Commun*. 2020;11:1875.
- Garretti F, Monahan C, Sette A, Agalliu D, Sulzer D. T cells, alpha-synuclein and Parkinson disease. *Handb Clin Neurol*. 2022;184:439–55.
- Sulzer D, Alcalay RN, Garretti F, Cote L, Kanter E, Agin-Liebes J, Liong C, McMurtrey C, Hildebrand WH, Mao X, Dawson VL, Dawson TM, Oseroff C, Pham J, Sidney J, Dillon MB, Carpenter C, Weiskopf D, Phillips E, Mallal S, Peters B, Frazier A, Lindestam CS, Arlehamn, Sette A. T cells from patients with Parkinson's disease recognize  $\alpha$ -synuclein peptides. *Nature*. 2017;546:656–61.
- Schonhoff AM, Williams GP, Wallen ZD, Standaert DG, Harms AS. Innate and adaptive immune responses in Parkinson's disease. *Prog Brain Res*. 2020;252:169–216.
- Wijeyekoon RS, Kronenberg-Versteeg D, Scott KM, Hayat S, Kuan WL, Evans JR, Breen DP, Cummins G, Jones JL, Clatworthy MR, Floto RA, Barker RA, and C. H. Williams-Gray. 2020. Peripheral innate immune and bacterial signals relate to clinical heterogeneity in Parkinson's disease. *Brain Behav Immun* 87:473–88.

18. Garretti F, Monahan C, Sloan N, Bergen J, Shahriar S, Kim SW, Sette A, Cutforth T, Kanter E, Agalliu D, Sulzer D. Interaction of an alpha-synuclein epitope with HLA-DRB1(\*)15:01 triggers enteric features in mice reminiscent of prodromal Parkinson's disease. *Neuron*. 2023;11:3397–413.
19. Sliter DA, Martinez J, Hao L, Chen X, Sun N, Fischer TD, Burman JL, Li Y, Zhang Z, Narendra DP, Cai H, Borsche M, Christine K, Youle RJ. Parkin and PINK1 mitigate STING-induced inflammation. *Nature*. 2018;561:258–62.
20. Hollenbach JA, Norman PJ, Creary LE, Damotte V, Montero-Martin G, Caillier S, Anderson KM, Misra MK, Nemat-Gorgani N, Osoegawa K, Santaniello A, Renschen A, Marin WM, Dandekar R, Parham P, Tanner CM, Hauser SL, Fernandez-Vina M, and J. R. Oksenberg. 2019. A specific amino acid motif of HLA-DRB1 mediates risk and interacts with smoking history in Parkinson's disease. *Proc Natl Acad Sci USA* 116: 7419–24.
21. Garretti F, Agalliu D, Lindestam Arlehamn CS, Sette A, Sulzer D. Autoimmunity in Parkinson's Disease: the role of alpha-synuclein-specific T cells. *Front Immunol*. 2019;10:303.
22. Bhatia D, Grozdanov V, Ruf WP, Kassubek J, Ludolph AC, Weishaupt JH, Danzer KM. T-cell dysregulation is associated with disease severity in Parkinson's Disease. *J Neuroinflammation*. 2021;18:250.
23. Scott KM, Chong YT, Park S, Wijeyekoon RS, Hayat S, Mathews RJ, Fitzpatrick Z, Tyers P, Wright G, Whitby J, Barker RA, Hu MT, Williams-Gray CH, Clatworthy MR. B lymphocyte responses in Parkinson's disease and their possible significance in disease progression. *Brain Commun*. 2023;5:fcad060.
24. Yan Z, Yang W, Wei H, Dean MN, Standaert DG, Cutter GR, Benveniste EN, Qin H. Dysregulation of the adaptive immune system in patients with early-stage Parkinson Disease. *Neuro Immunol Neuroinflamm*. 2021;8:e1036.
25. Villarino AV, Kanno Y, O'Shea JJ. Mechanisms and consequences of Jak-STAT signaling in the immune system. *Nat Immunol*. 2017;18:374–84.
26. Phillips RL, Wang Y, Cheon H, Kanno Y, Gadina M, Sartorelli V, Horvath CM, Darnell JE Jr, Stark GR, and J. J. O'Shea. 2022. The JAK-STAT pathway at 30: Much learned, much more to do. *Cell* 185: 3857–76.
27. O'Shea JJ, Schwartz DM, Villarino AV, Gadina M, McInnes IB, Laurence A. The JAK-STAT pathway: impact on human disease and therapeutic intervention. *Annu Rev Med*. 2015;66:311–28.
28. Yan Z, Gibson SA, Buckley JA, Qin H, Benveniste EN. 2016. Role of the JAK/STAT signaling pathway in regulation of innate immunity in neuroinflammatory diseases. *Clin Immunol pii: S1521–6616 (16) 30449–1*.
29. Jain M, Singh MK, Shyam H, Mishra A, Kumar S, Kumar A, Kushwaha J. Role of JAK/STAT in the neuroinflammation and its association with neurological disorders. *Ann Neurosci*. 2021;28:191–200.
30. Liu Y, Holdbrooks AT, De Sarno P, Rowse AL, Yanagisawa LL, McFarland BC, Harrington LE, Raman C, Sabbaj S, Benveniste EN, Qin H. Therapeutic efficacy of suppressing the JAK/STAT pathway in multiple models of experimental autoimmune encephalomyelitis. *J Immunol*. 2014;192:59–72.
31. Qin H, Buckley JA, Li X, Liu Y, Fox TH, Meares GP, Yu H, Yan Z, Harms AS, Li Y, Standaert DG, Benveniste EN. Inhibition of the JAK/STAT pathway protects against  $\alpha$ -synuclein-induced neuroinflammation and dopaminergic neurodegeneration. *J Neurosci*. 2016;36:5144–59.
32. Chesselet MF, Richter F, Zhu C, Magen I, Watson MB, Subramaniam SR. A progressive mouse model of Parkinson's disease: the Thy1-aSyn (line 61) mice. *Neurotherapeutics: J Exp Neurother*. 2012;9:297–314.
33. Rockenstein E, Mallory M, Hashimoto M, Song D, Shults CW, Lang I, Masliah E. Differential neuropathological alterations in transgenic mice expressing alpha-synuclein from the platelet-derived growth factor and Thy-1 promoters. *J Neurosci Res*. 2002;68:568–78.
34. Watson MB, Richter F, Lee SK, Gabby L, Wu J, Masliah E, Effros RB, Chesselet MF. Regionally-specific microglial activation in young mice over-expressing human wildtype alpha-synuclein. *Exp Neurol*. 2012;237:318–34.
35. Luk KC, Kehm V, Carroll J, Zhang B, O'Brien P, Trojanowski JQ, Lee VM. Pathological alpha-synuclein transmission initiates Parkinson-like neurodegeneration in nontransgenic mice. *Science*. 2012;338:949–53.
36. Luk KC, Kehm VM, Zhang B, O'Brien P, Trojanowski JQ, Lee VMY. Intra-cerebral inoculation of pathological alpha-synuclein initiates a rapidly progressive neurodegenerative alpha-synucleinopathy in mice. *J Exp Med*. 2012;209:975–86.
37. Richter F, Stanojlovic M, Kaufer C, Gericke B, Feja M. A mouse model to test novel therapeutics for Parkinson's Disease: an update on the Thy1-aSyn (line 61) mice. *Neurotherapeutics*. 2023;20:97–116.
38. Mahoney-Crane CL, Viswanathan M, Russell D, Curtiss RAC, Freire J, Bobba SS, Coyle SD, Kandebo M, Yao L, Wan BL, Hatcher NG, Smith SM, Marcus JN, Volpicelli-Daley LA. Neuronopathic GBA1L444P mutation accelerates glucosylsphingosine levels and formation of hippocampal alpha-synuclein inclusions. *J Neurosci*. 2023;43:501–21.
39. Stoyka LE, Arrant AE, Thrasher DR, Russell DL, Freire J, Mahoney CL, Narayanan A, Dib AG, Standaert DG, Volpicelli-Daley LA. Behavioral defects associated with amygdala and cortical dysfunction in mice with seeded alpha-synuclein inclusions. *Neurobiol Dis*. 2020;134:104708.
40. Abdelmotilib H, Maltbie T, Delic V, Liu Z, Hu X, Fraser KB, Moehle MS, Stoyka L, Anabtawi N, Krendelchtchikova V, Volpicelli-Daley LA, West A. Alpha-synuclein fibril-induced inclusion spread in rats and mice correlates with dopaminergic neurodegeneration. *Neurobiol Dis*. 2017;105:84–98.
41. Yan Z, Yang W, Parkitny L, Gibson SA, Lee KS, Collins F, Deshane JS, Cheng W, Weinmann AS, Wei H, Qin H, Benveniste EN. Deficiency of Socs3 leads to brain-targeted EAE via enhanced neutrophil activation and ROS production. *JCI Insight*. 2019;5:e126520.
42. Qin H, Holdbrooks AT, Liu Y, Reynolds SL, Yanagisawa LL, Benveniste EN. SOCS3 deficiency promotes M1 macrophage polarization and inflammation. *J Immunol*. 2012;189:3439–48.
43. Eisenstein M. Single-cell RNA-seq analysis software providers scramble to offer solutions. *Nat Biotechnol*. 2020;38:254–7.
44. Andueza A, Kumar S, Kim J, Kang DW, Mumme HL, Perez JJ, Villa-Roel N, Jo H. Endothelial reprogramming by disturbed Flow revealed by single-cell RNA and chromatin accessibility study. *Cell Rep*. 2020;33:108491.
45. Luecken MD, Theis FJ. Current best practices in single-cell RNA-seq analysis: a tutorial. *Mol Syst Biol*. 2019;15:e8746.
46. Heumos L, Schaar AC, Lance C, Litinetskaya A, Drost F, Zappia L, Lucken MD, Strobl DC, Henao J, Curion F, Single-cell Best Practices C, Schiller HB, Theis FJ. Best practices for single-cell analysis across modalities. *Nat Rev Genet*. 2023;24:550–72.
47. Greathouse KL, White JR, Vargas AJ, Bliskovsky VV, Beck JA, von Muhlinen N, Polley EC, Bowman ED, Khan MA, Robles AI, Cooks T, Ryan BM, Padgett N, Dzutsev AH, Trinchieri G, Pineda MA, Bilke S, Meltzer PS, Hokenstad AN, Stickrod TM, Walther-Antonio MR, Earl JP, Mell JC, Krol JE, Balashov SV, Bhat AS, Ehrlich GD, Valm A, Deming C, Conlan S, Oh J, Segre JA, Harris CC. Interaction between the microbiome and TP53 in human lung cancer. *Genome Biol*. 2018;19:123.
48. Hafemeister C, Satija R. Normalization and variance stabilization of single-cell RNA-seq data using regularized negative binomial regression. *Genome Biol*. 2019;20:296.
49. Subramanian A, Tamayo P, Mootha VK, Mukherjee S, Ebert BL, Gillette MA, Paulovich A, Pomeroy SL, Golub TR, Lander ES, Mesirov JP. Gene set enrichment analysis: a knowledge-based approach for interpreting genome-wide expression profiles. *Proc Natl Acad Sci USA*. 2005;102:15545–50.
50. McGeer PL, Itagaki S, Boyes BE, McGeer EG. Reactive microglia are positive for HLA-DR in the substantia nigra of Parkinson's and Alzheimer's disease brains. *Neurology*. 1988;38:1285–91.
51. Harms AS, Delic V, Thome AD, Bryant N, Liu Z, Chandra S, Jurkuvenaite A, West AB. Alpha-synuclein fibrils recruit peripheral immune cells in the rat brain prior to neurodegeneration. *Acta Neuropathol Commun*. 2017;5:85.
52. Stoyka LE, Mahoney CL, Thrasher DR, Russell DL, Cook AK, Harris AT, Narayanan A, Janado TP, Standaert DG, Roberson ED, Volpicelli-Daley LA. Templated alpha-synuclein inclusion formation is independent of endogenous tau. *eNeuro*. 2021;8:1–15.
53. Liu Y, Gibson SA, Benveniste EN, Qin H. Opportunities for translation from the bench: therapeutic intervention of the JAK/STAT pathway in neuroinflammatory diseases. *Crit Rev Immunol*. 2015;35:505–27.
54. Huang J, Liu L, Qin L, Huang H, Li X. Single-cell transcriptomics uncovers cellular heterogeneity, mechanisms, and therapeutic targets for Parkinson's Disease. *Front Genet*. 2022;13:686739.
55. Martirosyan A, Ansari R, Pestana F, Hebestreit K, Gasparyan H, Aleksanyan R, Hnatova S, Poovathingal S, Marneffe C, Thal DR, Kottick A, Hanson-Smith VJ, Guelfi S, Plumbly W, Belgard TG, Metzakopian E, Holt MG. Unravelling cell type-specific responses to Parkinson's Disease at single cell resolution. *Mol Neurodegener*. 2024;19:7.
56. Yan S, Si Y, Zhou W, Cheng R, Wang P, Wang D, Ding W, Shi W, Jiang Q, Yang F, Yao L. Single-cell transcriptomics reveals the interaction between peripheral CD4(+) CTLs and mesencephalic endothelial cells mediated by IFNG in Parkinson's disease. *Comput Biol Med*. 2023;158:106801.
57. Kamath T, Abdurouaf A, Burris SJ, Langlieb J, Gazestani V, Nadaf NM, Balderama K, Vanderburg C, Macosko EZ. Single-cell genomic profiling of human dopamine neurons identifies a population that selectively degenerates in Parkinson's disease. *Nat Neurosci*. 2022;25:588–95.



58. Barman PK, Shin JE, Lewis SA, Kang S, Wu D, Wang Y, Yang X, Nagarkatti PS, Nagarkatti M, Messaoudi I, Benayoun BA, and H. S. Goodridge. 2022. Production of MHCII-expressing classical monocytes increases during aging in mice and humans. *Aging Cell* 21: e13701.
59. Kambey PA, Liu WY, Wu J, Bosco B, Nadeem I, Kanwore K, Gao DS. Single-nuclei RNA sequencing uncovers heterogeneous transcriptional signatures in Parkinson's disease associated with nuclear receptor-related factor 1 defect. *Neural Regen Res*. 2023;18:2037–46.
60. Schonhoff AM, Figue DA, Williams GP, Jurkuvenaite A, Gallups NJ, Childers GM, Webster JM, Standaert DG, Goldman JE, Harms AS. Border-associated macrophages mediate the neuroinflammatory response in an alpha-synuclein model of Parkinson disease. *Nat Commun*. 2023;14:3754.
61. Xi K, Cai SQ, Yan HF, Tian Y, Cai J, Yang XM, Wang JM, Xing GG. CSMD3 deficiency leads to motor impairments and autism-like behaviors via dysfunction of cerebellar purkinje cells in mice. *J Neurosci*. 2023;43:3949–69.
62. Floris C, Rasmu S, Boccone L, Gasperini D, Cao A, Crisponi L. Two patients with balanced translocations and autistic disorder: CSMD3 as a candidate gene for autism found in their common 8q23 breakpoint area. *Eur J Hum Genet*. 2008;16:696–704.
63. Li M, Wang Z, Dong S, Xu Y. 2022. NAV3 Is a Novel Prognostic Biomarker Affecting the Immune Status of the Tumor Microenvironment in Colorectal Cancer. *J Immunol Res* 2022: 8337048.
64. Zhou X, Feliciano P, Shu C, Wang T, Astrovskaya I, Hall JB, Obajulu JU, Wright JR, Murali SC, Xu SX, Brueggeman L, Thomas TR, Marchenko O, Fleisch C, Barns SD, Snyder LG, Han B, Chang TS, Turner TN, Harvey WT, Nishida A, O'Roak BJ, Geschwind DH, Consortium S, Michaelson JJ, Volfovsky N, Eichler EE, Shen Y, Chung WK. Integrating de novo and inherited variants in 42,607 autism cases identifies mutations in new moderate-risk genes. *Nat Genet*. 2022;54:1305–19.
65. Cui H, Banerjee S, Guo S, Xie N, Ge J, Jiang D, Zornig M, Thannickal VJ, Liu G. Long noncoding RNA Malat1 regulates differential activation of macrophages and response to lung injury. *JCI Insight*. 2019;4(4):e124522.
66. Shu B, Zhou YX, Li H, Zhang RZ, He C, Yang X. The METTL3/MALAT1/PTBP1/USP8/TAK1 axis promotes pyroptosis and M1 polarization of macrophages and contributes to liver fibrosis. *Cell Death Discov*. 2021;7:368.
67. Sanchez-Guajardo V, Tentillier N, Romero-Ramos M. The relation between alpha-synuclein and microglia in Parkinson's disease: recent developments. *Neuroscience*. 2015;302:47–58.
68. Xu J, Farsad HL, Hou Y, Barclay K, Lopez BA, Yamada S, Saliu IO, Shi Y, Knight WC, Bateman RJ, Benzinger TLS, Yi JJ, Li Q, Wang T, Perlmutter JS, Morris JC, Zhao G. Human striatal glia differentially contribute to AD- and PD-specific neurodegeneration. *Nat Aging*. 2023;3:346–65.
69. Grozdanov V, Bousset L, Hoffmeister M, Bliederhaeuser C, Meier C, Madiona K, Pieri L, Kiechle M, McLean PJ, Kassubek J, Behrends C, Ludolph AC, Weishaupt JH, Melki R, Danzer KM. Increased immune activation by pathologic alpha-synuclein in Parkinson's Disease. *Ann Neurol*. 2019;86:593–606.
70. Kuhns MS, Badgandi HB. Piecing together the family portrait of TCR-CD3 complexes. *Immunol Rev*. 2012;250:120–43.
71. Ho IC, Tai TS, Pai SY. GATA3 and the T-cell lineage: essential functions before and after T-helper-2-cell differentiation. *Nat Rev Immunol*. 2009;9:125–35.
72. Tindemans I, Serafini N, Di Santo JP, Hendriks RW. GATA-3 function in innate and adaptive immunity. *Immunity*. 2014;41:191–206.
73. Valitutti S, Muller S, Salio M, Lanzavecchia A. Degradation of T cell receptor (TCR)-CD3-zeta complexes after antigenic stimulation. *J Exp Med*. 1997;185:1859–64.
74. Liu H, Rhodes M, Wiest DL, Vignali DA. On the dynamics of TCR:CD3 complex cell surface expression and downmodulation. *Immunity*. 2000;13:665–75.
75. Zheng W, Flavell RA. The transcription factor GATA-3 is necessary and sufficient for Th2 cytokine gene expression in CD4 T cells. *Cell*. 1997;89:587–96.
76. Potter SS. Single-cell RNA sequencing for the study of development, physiology and disease. *Nat Rev Nephrol*. 2018;14:479–92.
77. Shapiro E, Biezuner T, Linnarsson S. Single-cell sequencing-based technologies will revolutionize whole-organism science. *Nat Rev Genet*. 2013;14:618–30.
78. Kharchenko PV. The triumphs and limitations of computational methods for scRNA-seq. *Nat Methods*. 2021;18:723–32.
79. Wang R, Li M, Ding Q, Cai J, Yu Y, Liu X, Mao J, Zhu YZ. Neuron navigator 2 is a novel mediator of rheumatoid arthritis. *Cell Mol Immunol*. 2021;18:2288–9.
80. Wang R, Cai J, Chen K, Zhu M, Li Z, Liu H, Liu T, Mao J, Ding Q, Zhu YZ. STAT3-NAV2 axis as a new therapeutic target for rheumatoid arthritis via activating SSH1L/Cofilin-1 signaling pathway. *Signal Transduct Target Ther*. 2022;7:209.
81. Wang KS, Liu Y, Xu C, Liu X, Luo X. Family-based association analysis of NAV2 gene with the risk and age at onset of Alzheimer's disease. *J Neuroimmunol*. 2017;310:60–5.
82. Silvin A, Uderhardt S, Piot C, Da Mesquita S, Yang K, Geirsdottir L, Mulder K, Eyal D, Liu Z, Bridance C, Thion MS, Zhang XM, Kong WT, Deloger M, Fontes V, Weiner A, Ee R, Dress R, Hang JW, Balachander A, Chakarov S, Malleret B, Dunsmore G, Cexus O, Chen J, Garel S, Dutertre CA, Amit I, Kipnis J, Ginhoux F. Dual ontogeny of disease-associated microglia and disease inflammatory macrophages in aging and neurodegeneration. *Immunity*. 2022;55:1448–65.
83. Silvin A, Qian J, Ginhoux F. Brain macrophage development, diversity and dysregulation in health and disease. *Cell Mol Immunol*. 2023;20:1277–89.
84. De Vlaminck K, Van Hove H, Kancheva D, Scheyltjens I, Pombo Antunes AR, Bastos J, Vara-Perez M, Ali L, Mampay M, Deneyer L, Miranda JF, Cai R, Bouwens L, De Bundel D, Caljon G, Stijlemans B, Massie A, Van Ginderachter JA, Vandembroucke RE, Movahedi K. Differential plasticity and fate of brain-resident and recruited macrophages during the onset and resolution of neuroinflammation. *Immunity*. 2022;55:2085–102.
85. Parhizkar S, Holtzman DM. APOE mediated neuroinflammation and neurodegeneration in Alzheimer's disease. *Semin Immunol*. 2022;59:101594.
86. Kloske CM, Wilcock DM. The important interface between apolipoprotein E and neuroinflammation in Alzheimer's Disease. *Front Immunol*. 2020;11:754.
87. Mata IF, Leverenz JB, Weintraub D, Trojanowski JQ, Hurtig HI, Van Deerlin VM, Ritz B, Rausch R, Rhodes SL, Factor SA, Wood-Siviero C, Quinn JF, Chung KA, Peterson AL, Espay AJ, Revilla FJ, Devoto J, Hu SC, Cholerton BA, Wan JY, Montine TJ, Edwards KL, Zabetian CP. APOE, MAPT, and SNCA genes and cognitive performance in Parkinson disease. *JAMA Neurol*. 2014;71:1405–12.
88. Guerreiro R, Ross OA, Kun-Rodrigues C, Hernandez DG, Orme T, Eicher JD, Shepherd CE, Parkkinen L, Darwent L, Heckman MG, Scholz SW, Troncoso JC, Pletnikova O, Ansoorge O, Clarimon J, Lleo A, Morenas-Rodriguez E, Clark L, Honig LS, Marder K, Lemstra A, Rogaeva E, George-Hyslop PS, Londo E, Zetterberg H, Barber I, Braae A, Brown K, Morgan K, Troakes C, Al-Sarraj S, Lashley T, Holton J, Compta Y, Van Deerlin V, Serrano GE, Beach TG, Lesage S, Galasko D, Masliah E, Santana I, Pastor P, Diez-Fairen M, Aguilar M, Tienari PJ, Myllykangas L, Oinas M, Revez T, Lees A, Boeve BF, Petersen RC, Ferman TJ, Escott-Price V, Graff-Radford N, Cairns NJ, Morris JC, Pickering-Brown S, Mann D, Halliday GM, Hardy J, J. Q., Trojanowski DW, Dickson A, Singleton DJ, Stone, Bras J. 2018. Investigating the genetic architecture of dementia with Lewy bodies: a two-stage genome-wide association study. *Lancet Neurol* 17: 64–74.
89. Davis AA, Inman CE, Wargel ZM, Dube U, Freeberg BM, Galluppi A, Haines JN, Dhavale DD, Miller R, Choudhury FA, Sullivan PM, Cruchaga C, Perlmutter JS, Ulrich JD, Benitez BA, Kotzbauer PT, Holtzman DM. APOE genotype regulates pathology and disease progression in synucleinopathy. *Sci Transl Med*. 2020;12:eaay3069.
90. Zhao N, Attrebi ON, Ren Y, Qiao W, Sonustun B, Martens YA, Meneses AD, Li F, Shue F, Zheng J, Van Ingelgom AJ, Davis MD, Kurti A, Knight JA, Linares C, Chen Y, Delenclos M, Liu CC, Fryer JD, Asmann YW, McLean PJ, Dickson DW, Ross OA, Bu G. APOE4 exacerbates alpha-synuclein pathology and related toxicity independent of amyloid. *Sci Transl Med*. 2020;12:eaay1809.
91. Capelle CM, Cire S, Hedin F, Hansen M, Pavelka L, Grzyb K, Kyriakis D, Hunewald O, Konstantinou M, Revets D, Tslaf V, Marques TM, Gomes CPC, Baron A, Domingues O, Gomez M, Zeng N, Betsou F, May P, Skupin A, Cosma A, Balling R, Kruger R, Ollert M, Hefeng FQ. Early-to-mid stage idiopathic Parkinson's disease shows enhanced cytotoxicity and differentiation in CD8 T-cells in females. *Nat Commun*. 2023;14:7461.
92. Wang P, Yao L, Luo M, Zhou W, Jin X, Xu Z, Yan S, Li Y, Xu C, Cheng R, Huang Y, Lin X, Ma K, Cao H, Liu H, Xue G, Han F, Nie H, Jiang Q. Single-cell transcriptome and TCR profiling reveal activated and expanded T cell populations in Parkinson's disease. *Cell Discov*. 2021;7:52.
93. Acharya S, Lumley AI, Zhang L, Vausort M, Devaux Y, On Behalf Of The Ncer-Pd Consortium. GATA3 as a blood-based RNA biomarker for idiopathic Parkinson's Disease. *Int J Mol Sci*. 2023;24:10040.
94. Kustrimovic N, Comi C, Magistrelli L, Rasini E, Legnaro M, Bombelli R, Aleksic I, Blandini F, Minafra B, Riboldazzi G, Sturchio A, Mauri M, Bono G, Marino F, Cosentino M. Parkinson's disease patients have a complex phenotypic and functional Th1 bias: cross-sectional studies of CD4+Th1/Th2/T17 and Treg in drug-naive and drug-treated patients. *J Neuroinflammation*. 2018;15:205.
95. Czimmerer Z, Daniel B, Horvath A, Ruckerl D, Nagy G, Kiss M, Peloquin M, Budai MM, Cuaranta-Monroy I, Simandi Z, Steiner L, Nagy B Jr., Poliska S, Banko C, Bacso Z, Schulman IG, Sauer S, Deleuze JF, Allen JE, Benko S, Nagy L. The transcription factor STAT6 mediates direct repression of inflammatory enhancers and limits activation of alternatively polarized macrophages. *Immunity*. 2018;48:75–90. e76.

96. Seif F, Khoshmirsafa M, Aazami H, Mohsenzadegan M, Sedighi G, Bahar M. The role of JAK-STAT signaling pathway and its regulators in the fate of T helper cells. *Cell Commun Signal*. 2017;15:23.
97. Egwuagu CE. STAT3 in CD4+T helper cell differentiation and inflammatory diseases. *Cytokine*. 2009;47:149–56.
98. Durant L, Watford WT, Ramos HL, Laurence A, Vahedi G, Wei L, Takahashi H, Sun HW, Kanno Y, Powrie F, and J. J. O'Shea. 2010. Diverse targets of the transcription factor STAT3 contribute to T cell pathogenicity and homeostasis. *Immunity* 32: 605–15.
99. Priceman SJ, Kujawski M, Shen S, Cherryholmes GA, Lee H, Zhang C, Kruper L, Mortimer J, Jove R, Riggs AD, and H. Yu. Regulation of adipose tissue T cell subsets by Stat3 is crucial for diet-induced obesity and insulin resistance. *Proc Natl Acad Sci USA*. 2013;110:13079–84.
100. Deenick EK, Pelham SJ, Kane A, Ma CS. Signal transducer and activator of transcription 3 control of human T and B cell responses. *Front Immunol*. 2018;9:168.
101. Iba M, Kim C, Sallin M, Kwon S, Verma A, Overk C, Rissman RA, Sen R, Sen JM, Masliah E. Neuroinflammation is associated with infiltration of T cells in Lewy body disease and alpha-synuclein transgenic models. *J Neuroinflammation*. 2020;17:214.

### **Publisher's note**

Springer Nature remains neutral with regard to jurisdictional claims in published maps and institutional affiliations.